

FIRST EDITION

IONOSPHERIC
PROPAGATION USING
HIGH FREQUENCY
RADIO SIGNALS

PROJECT NOTES

MAXWELL MORAN
W3LLA



Table of Contents

Sections

I. Introduction	6
A. Motivation	6
B. Personal Note	7
II. Ionospheric Propagation	9
A. Abstract	9
B. Background	9
C. Virtual Height	17
D. Take-off Angles and the Ionization Layers – A Simplified Model	19
E. Snell’s Law of Refraction	20
F. Critical Frequency	22
G. Maximum Usable Frequency	24
H. Expanded Model	26
I. Effective Earth Radius and Skip Distance	31
J. Validating the Effective Earth Radius Using the Expanded Model	33
K. Ionosphere Tracking Models	36
III. Visualizing the Ionosphere Using the Weak Signal Propagation Reporter	41
A. Introduction	41
B. Why WSPR? Narrow Bandwidth and Reduced Power: A Quick Primer	42
C. Experiment – 20m Propagation Analysis	48
D. Results and Commentary	48
E. WSPR Propagation in Relation to Ionosonde Critical Frequency Readings	52
F. Heat Mapping WSPR Data	57
IV. Signal Propagation Mathematics – Colorado State University Project	63
A. Overview	63
B. Hypothesis	63
C. Construct	63
D. Model	64
E. Transmit	64
F. Analyze	65
G. Antenna Modeling	66
H. WSPR Background	68

I.	WSPR Field Test Results	70
J.	Summary Conclusions	71
V.	Modification of the QRP Labs QCX CW Transceiver	72
A.	Introduction	72
B.	Motivation	72
C.	Overview of Design Specifics that Limit the Receive Capability on WSPR	73
D.	CW Filter Bypass Modification	74
VI.	References	79

List of Figures and Tables

List of Figures

Figure 1:	Electromagnetic Wave	9
Figure 2:	Illustrated ionospheric layers	10
Figure 3:	Illustrative Ionospheric	12
Figure 4:	Illustrative diurnal changes in the ionosphere	13
Figure 5:	Illustrative electron density at solar maximum and minimum with diurnal impacts	14
Figure 6:	Illustrative take-off angles & angles of incidence	16
Figure 7:	Virtual height	17
Figure 8:	Layered Conceptualization of the Ionosphere (3; 20)	17
Figure 9:	Vertical incidence	18
Figure 10:	Simplified geometric ionospheric model	19
Figure 11:	Angles of incidence and refraction	20
Figure 12:	Illustrative ionosphere electron density profile	23
Figure 13:	Expanded ionospheric model	26
Figure 14:	Amended NOAA electron density profile	27
Figure 15:	Expanded ionospheric model with take-off angles $>0^\circ$	29
Figure 16:	Straight path maximum distance using r_e with a 0° take-off angle	32
Figure 17:	Curved path maximum distance using r_e with a 0° take-off angle	34
Figure 18:	Ionospheric electron density at sunspot maximum - illustrative	35
Figure 19:	Real time total electron count map	36
Figure 20:	Real time foF2 (Critical Frequency)	37
Figure 21:	NOAA worldwide vertical ionosonde network – 130 Stations	38
Figure 22:	Illustrative ionogram report – June 15 2019	38
Figure 23:	Calculated Plasma Frequency – June 15 2019 Boulder Station using IRI Data	39
Figure 24:	Calculated plasma frequency & MuF at various take-off angles 6/15/19 Boulder Station using IRI data	40
Figure 25:	WSPR transmissions (W3LLA, 1/31/20 to 2/1/20) - Spots	48
Figure 26:	WSPR 24 Hour transmissions (W3LLA, 1/31/20 to 2/1/20) - Distance vs time (local time)	49
Figure 27:	WSPR 24 Hour transmissions (W3LLA, 1/31/20 to 2/1/20) – Count per sequence vs time (local time)	50
Figure 28:	WSPR 24 Hour transmissions (W3LLA, 1/31/20 to 2/1/20) - Average distance (km) per sequence vs time (local time)	51
Figure 29:	Illustrative Ionogram from Boulder station	53

Figure 30:	Boulder Station Ionospheric Layer Heights (local time)	53
Figure 31:	Boulder Station Ionospheric Layer Heights with Composite Height (local time)	54
Figure 32:	WSPR 24 Hour Spots (3/6/20 to 3/7/20) Against Composite Ionospheric Height (km)	54
Figure 33:	WSPR 24 Hour transmissions (W3LLA, 3/6/20 to 3/7/20) - Distance vs time (local time)	55
Figure 34:	WSPR 24 Hour transmissions (W3LLA, 3/6/20 to 3/7/20) – Average Spot Distance per Transmission Sequence and Composite Ionospheric Height vs time (local time)	56
Figure 35:	WSPR transmissions (W3LLA, 2/28/20 to 2/29/20) - 24 Hour Spots	57
Figure 36:	WSPR transmissions (W3LLA, 2/28/20 to 2/29/20) - 24 Hour Heat Map	58
Figure 37:	Sun Tracking Path (Ft. Collins, CO 2/28/20 to 2/29/20)	59
Figure 38:	WSPR 24 Hour transmissions (W3LLA, 2/28/20 to 2/29/20) – Mid Point Spot Heat Cluster (local time)	62
Figure 39:	3D view – dipole antenna	64
Figure 40:	QRP Labs, QCX Transceiver	65
Figure 41:	Decibel relation to power ratio	66
Figure 42:	3D view of the propagation pattern of a dipole at different heights	66
Figure 43:	Antenna radiation patterns at different heights	67
Figure 44:	Total WSPR spots 20m band	69
Figure 45:	Total WSPR Spots at $1/8 \lambda$ (Low Height) – KM & Azimuth	70
Figure 46:	Total WSPR Spots at $1/3 \lambda$ (High Height) – KM & Azimuth	70
Figure 47:	QCX 200Hz CW Filter	73
Figure 48:	Audio frequency range of CW vs WSPR modes	74
Figure 49:	CF filter bypass modification schematics	75
Figure 50:	CF filter bypass modification - highlighted components	76
Figure 51:	PCB track schematic - common nodes into R27	76
Figure 52:	R59 with orientation changed (left) and jumper attached (right)	77
Figure 53:	C20 with one end connected to PCB and the wire attached to lead (left) and completed modification (right)	78
Figure 54:	Illustrative reception reports post modification – 2/2/2019, 20m band	78

List of Tables

Table 1:	Expanded Model - 0° take-off angle	28
Table 2:	Expanded Model - 30° take-off angle	30
Table 3:	Expanded Model – propagation matrix	30
Table 4:	Expanded Model using IRI electron density figures at Boulder Station (6/15/19)	40
Table 5:	Example spreadsheet calculation	69
Table 6:	Field test results	71

I. Introduction

A. Motivation

Why should anyone bother with Amateur Radio in an era of smart phones and internet based voice, video, and data communication? Why would anyone want to use a radio and a large antenna to contact Europe or Australia when you can just access your WhatsApp? Why is amateur radio of interest to me? For me, there is something almost primal about amateur radio. I find it fascinating that with a simple copper wire and a homebrew transmitter, I can bounce a signal off of the ionosphere and reach stations thousands of miles away, such as Antarctica. Radio waves can even be bounced off of the moon and travel back to Earth. I compare the allure of Amateur Radio to the thrill of sailing the seas on a sailboat using wind power alone. Similarly to amateur radio in communication, sailing boats are no longer the primary source of transportation. Yet, when we watch yacht races or spot a schooner on the horizon we are mesmerized by the majesty and mystique of its massive masts and sails full of wind. Like the sailing boats, Amateur Radio prevailed despite the numerous technological advances. Even the invention of computers did not derail Amateur Radio but greatly enhanced it.

Radio communication which uses electromagnetic waves requires experience and advanced knowledge. Communication using high frequency (HF) radio waves in the range of 3-30MHz is generally characterized as either ground wave, space (air) wave, or sky wave (ionospheric).

Groundwave propagation is when a radio signal travels along the surface of the Earth, and it is characterized by high levels of signal attenuation across the surface; as a result, communication distance is limited.

Space (air) wave propagation refers to communication where radio signals travel directly from a transmitter to a receiving station via Line of Sight (LoS) communications link. LoS communications on Earth are restricted by the horizon and antenna height. As result, typical communication distances are limited to approximately 15% beyond the visible horizon in the case of handheld VHF radios or to 10km for an antenna mast 3 meters high^[1].

Sky wave propagation refers to signals in a communications circuit that are propagated through the ionosphere. Sky wave propagation is also the focus of this report. HF sky wave communication has the ability to communicate voice and data around the world without relying on an extensive and expensive communication infrastructure like satellites, cell towers, or cable networks. This form of communication

[1] Calculated using Equation [58] for an assumed height of 1.7m and 3.3m for handheld and antenna mast heights respectively vs a visible horizon assumed to be 4.7km

has the ability to mitigate many of the limitations of groundwave and line of sight communications by using the ionosphere to overcome land obstacles such as mountains or valleys, and it is not impeded by ground loss (1).

Similar to sailing, communicating by air is an art. At any particular moment in time, radio signals are either absorbed, refracted, or they pass through the ionosphere depending upon their wavelength and their angle of incidence as they enter the ionosphere. Fluctuations in the ionosphere are both regular and random, and understanding ionospheric conditions is as important to a radio operator as the Beaufort scale is to a ship's captain at sea. The nautical term "rig", which The Oxford Encyclopedic English Dictionary defines as "the arrangement of masts, sails, etc. of a sailing ship", is also used by radio operators to describe their transceiver connected to an antenna. Those who have been on a sailing boat, can surely appreciate the incredible skills of experienced sailors who instinctively know how to fine tune their rig to sail the open seas.

Despite the simplicity and the benefits of HF sky wave communication, it remains unpredictable because the ionosphere itself is an ever-changing medium...just like the wind. The unpredictable nature of HF communication makes for a frustrating and rewarding pursuit, and knowledge of the interplay between frequency, power, take-off angles and ionospheric conditions can be a determining factor for successful communications links.

B. Personal Note

My fascination with radio communication started when I was quite young. Since my family's backyard in Colorado extends to an open wooded area, my parents gave me and my younger brother basic walkie-talkies so we could range outside and report back to them. In Poland, at the Baltic Sea, where we spend our summers, we were gifted similar walkie-talkies to use when playing outside. We started experimenting with how far we could go before we lost connection with our parents and got in trouble for going too far. Radio is useful in so many ways. When we sail the Baltic Sea with our family friends, the only way we can communicate with land and other vessels is by radio. Similarly, when we camp in the Rocky Mountains, the only way to communicate there is by radio. Because I always preferred to read math and scientific books rather than novels, I started researching radio communication and the ionosphere. I came across several explanations about how propagation works, but some of the math did not make sense to me. Some authors would either skip some steps (assuming a higher level of mathematical knowledge) or make some random approximations I did not understand. This forced me to dig deeper to search for answers.

This report is a result of my independent research on a number of topics relating to ionospheric propagation. It is a collection of my personal project notes and research summaries and a result of my ongoing effort at trying to understand radio propagation. It is a work in progress. In this report, I present

a number of mathematical models in great detail. I did this to keep my thoughts organized and to help me recall these concepts for later use. All of the references that have informed my analysis have been sourced from free and/or publicly available resources. In similar spirit (and in the spirit of Part 97 of the FCC rules pertaining to Amateur Radio Service), I am sharing my work in progress research to promote international goodwill, understanding, and cooperation, and I hope that others can benefit from my efforts.

I would like to thank my Elmer, Glenn Elmore (N6GN), for sharing his energy and knowledge, Roger Stevens (KK6EEW) who gifted me an old TS-440S HF radio, the radio community at large and all the hams from all over the world who have sent me e-mails of encouragement, and my mom for buying me a transceiver kit for Christmas. Special thanks for the countless hours of editorial services of both of my parents.

II. Ionospheric Propagation

A. Abstract

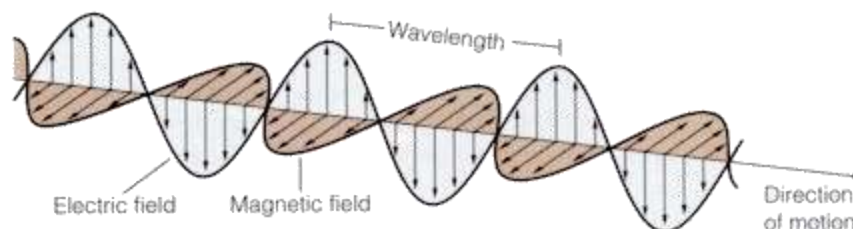
Using a steady-state, normalized ionospheric model, which assumes a defined level of electron density, a relationship between the electron density and frequency of a transmitted signal can be made (2; 3; 4). This relationship can be made by applying laws of refraction to the index of refraction for the ionospheric model, which determines the required frequencies for successful ionospheric skip propagation at varying angles of incidence a signal enters the ionosphere (2; 3). Once those frequencies are established, geometric relations can be applied to determine a theoretical take-off angle and single skip distance these radio waves can travel using a spherical earth model.

This report presents a brief summary of key concepts of an expanded propagation model which determines skip distances, critical frequencies, and maximum usable frequencies based on assumed take-off angles and electron densities at various altitudes and which applies a linear change gradient to the index of refraction of the ionosphere.

B. Background

Radio signals (RF signals/electromagnetic radiation) travel at the speed of light and in a wavelike pattern. These radio waves oscillate from peak to peak at a frequency that is measured in Hz (cycles per one second). High Frequency (HF) radio signals, the subject of this report, have a frequency in the range of 3MHz to 30 MHz (i.e. 3-30 million hertz per second).

Figure 1: Electromagnetic Wave



Source: <http://faculty.cord.edu/manning/physics215/studentpages/angieevanson.html>

The speed of light in a vacuum is approximately 300M meters per second, and a relationship between wavelength in meters (λ) and frequency (f) in MHz is (5):

$$c = \lambda \times f \quad [1]$$

Therefore, the wavelength of a signal in meters at a specific frequency in MHz can be determined to be

$$\lambda = \frac{c}{f} \quad [2]$$

Where:

c = Speed of light \cong 300M m/s

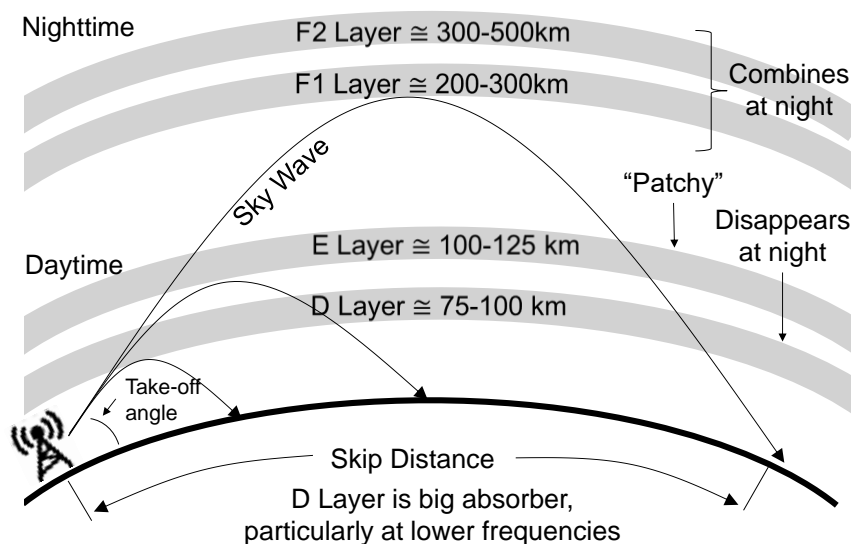
λ = wavelength in meters

f = frequency in MHz (10^6 cycles/second)

Amateur radio operators refer to radio signals by their frequency or by the wavelength in meters interchangeably, with a range of wavelengths signifying a particular band. For example, a 14MHz signal is determined to be a signal in the 20 meter band (i.e. $300M \text{ m/s} \div 14 \text{ MHz}$).

These electromagnetic waves are modulated in amplitude, phase and frequency at source with communication information imparted to the waveform and are demodulated by a receiving station. Because radio signals can be refracted back to Earth by the electrically charged layer of the upper atmosphere called the ionosphere (6), these HF signals travel great distances. HF signals in the range of 3 to 30 MHz are unique in their ability to utilize the ionosphere for long distance transmissions, and frequencies outside this range do not consistently support ionospheric propagation (7).

Figure 2: Illustrated ionospheric layers



Source: W3LLA with layer altitude indications provided by NOAA

Radio wave propagation using the ionosphere depends upon a number of interrelated factors, for example:

- **Ionospheric conditions** – The ionosphere is greatly impacted by the 11 year sunspot cycle, solar flares, and daytime (diurnal) solar radiation.
- **Transmission frequency** - At any given time and location, there is an ever changing maximum usable frequency (MuF) above which signals pass through into space, and there is a lowest usable frequency (LuF) below which signals are absorbed. Signal attenuation has a relationship to the frequency: the higher the frequency, the less attenuation.
- **Take-off angle** - 90° is directly overhead, and 0° is directed towards the horizon. As a rule of thumb, the lower the take-off angle that a signal is sent, the further it will travel, because it enters the ionosphere at a greater angle of incidence and at a greater distance from the signal's origin than if the signal was directed directly overhead.

While a number of other factors impact radio wave propagation, like the effect of ground, transmission power, feed point impedance, space weather, this analysis focuses on the geometric and frequency dynamics of ionospheric skip communication.

The Ionosphere

The formation of the ionosphere occurs in direct response to the impact of solar radiation on the upper regions of Earth's atmosphere. The solar radiation, primarily EUV and x-ray radiation, transfers its energy by heating the atmosphere in the region from 200 to 500 miles above the Earth by thousands of degrees. This process, called ionization, strips atoms of their electrons, which creates ions and negatively charged electrons. (8; 6; 9).

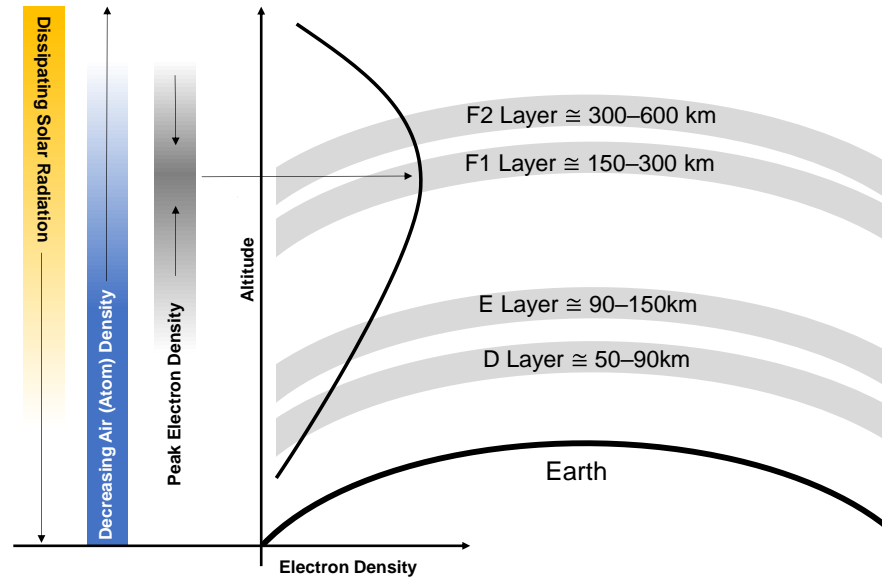
As solar radiation enters the Earth's atmosphere, the intensity of the radiation is highest at the higher altitudes. However, the air density is the lowest at these upper levels. Therefore, solar radiation ionizes an increasing amount of atoms as it moves to lower altitudes due to the increasing air density while transferring an increasing amount of energy along the way. This conceptualized representation of ionization production at various altitudes was presented by Sydney Chapman 1931.

At some point in its path, the energy required to ionize atoms becomes sufficiently dissipated in its downward journey that ionization begins to occur at a decreasing rate, and the production rate of electrons decreases (10).

This process of ionization occurs in the altitude region between 75km to 500km. While one thinks of the ionosphere as a distinct layer of the atmosphere, the ionosphere is, in fact, comprised of regions of

varying electron density, and the layers are considered to be peak ionization at different altitudes or concentrated layers of charged particles (8; 11)

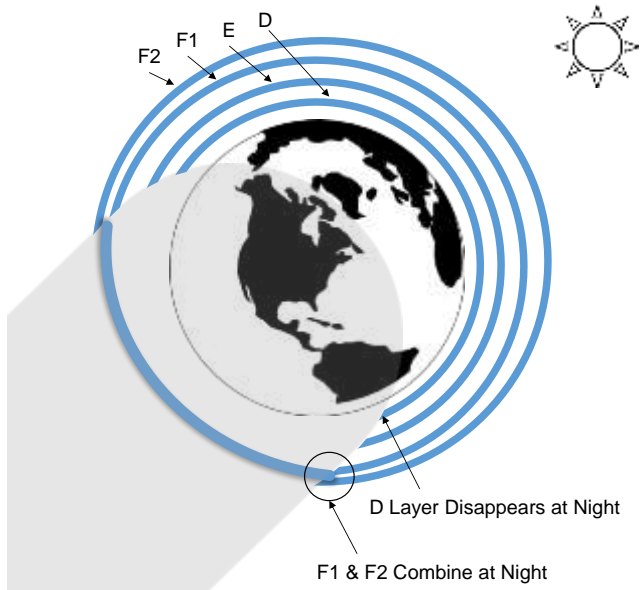
Figure 3: Illustrative Ionospheric



Source: W3LLA

Variations in the amount of solar radiation has an immediate and immense impact on the production rate of ions and the rate at which these free electrons recombine and reconstitute back into neutral particles (8; 10). These variations in solar radiation occur in relation to the 11 year solar cycle, solar activity like solar flares and, most prominently and predictably as a result of the diurnal changes resulting of the rising and setting of the Sun.

Figure 4: Illustrative diurnal changes in the ionosphere



Source: W3LLA, Adapted from (6)

The figure above illustrates how the sun facing regions of the Earth are subjected to the most solar radiation and that all the ionization layers are active. High frequency communications using the ionosphere during the daytime contend with multiple layers of ionization which attenuates signals. In particular, the presence of the D layer attenuates signals and limits skip distances given its lower altitude relative to the E, F1 and F2 Layers. In order to propagate a signal through the upper ionospheric layers, and thus achieve greater skip distances, higher frequencies are required to pass through the D Layer, provided that the signal frequency does not exceed a theoretical maximum frequency (Maximum Usable Frequency) for the higher layers above which the signal penetrates rather than refracts (6; 12).

Signal attenuation in the ionosphere has a relationship to the frequency of the signal being sent, electron density and air density. A signal propagating through the ionosphere imparts its oscillatory waveform to the free, negatively charged electrons which in turn act as a weak conductor causing those electrons to be moved a distance that is proportional to the wavelength (13; 12). This displacement of electrons expends energy in the process and a relationship is established where the longer the wavelength (i.e. the lower the frequency), the greater the distance the electron is moved and therefore more of the signal's energy is dissipated in the process while also increasing the likelihood that the free electrons will encounter and recombine with ions in the process (14).

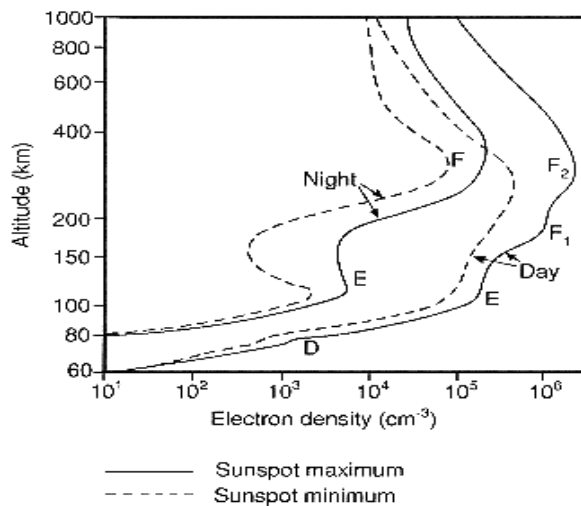
Higher concentrations of electrons also exacerbates the process of attenuation as the energy loss is amplified across a denser electron count. The greater electron density, the more likely a signal will be refracted, while at the same time, the higher the frequency, the less the signal will be subject to that refraction (12; 15). Similarly, the higher the electron density and the lower the signal frequency (i.e. the longer the wavelength), the more prone the signal is to being absorbed or attenuated during its path. Higher frequencies require higher electron densities to refract in comparison to lower frequencies.

In addition to the impact of frequency and electron density, attenuation is also impacted by air density. At lower altitudes, where there is higher air pressure, free electrons will have more collisions with more particles, and their energy will be dissipated. In this scenario, the longer the wavelength, the more collisions will occur per wavelength, thus attenuating lower frequencies more in relation to higher frequencies of shorter wavelength. At higher altitudes with a lower air density, there are less collisions with particles and therefore less attenuation from these collisions.

At night when there is no solar radiation, ionization (particularly in the D Layer) stops, and the free electrons and ions recombine at a faster rate than they are created and thus, electron density drops (16). This process of recombination happens at varying rates depending upon the altitude with typical lifetimes of charge particles lasting a few seconds in the lower D Layer, a few minutes in the E Layer, and up to an hour for the F Layers where the air is so thin (8). Accordingly, electron density in the D Layer collapses quickly after sunset which allows the lower frequency signals to reach F Layer.

In order to derive general properties about signal propagation using the ionosphere, a generalized model of the ionosphere is used in this presentation, which compares electron density (N) per cm^3 along an x-axis against altitude in kilometres along the y-axis. For simplicity purposes, the “Illustrative ionosphere electron density profile” outlined in Figure 12 (page 23) is used as a proxy for a normalized representation of the ionosphere in this presentation. However, it should be emphasized how volatile and extreme the electron density is in response to solar phenomena.

Figure 5: Illustrative electron density at solar maximum and minimum with diurnal impacts



Source: (17)

Transmission Frequency

Signal attenuation in the ionosphere, particularly at the lower D layer, can be so substantial that many of the low angle of take-off transmissions on the lower bands (i.e. MF and frequencies below 14MHz)

are absorbed during the day (12 pp. 8-3; 18). For transmissions during the daytime, signal attenuation within the D Layer is the inverse square of the frequency (6).

$$\text{Signal attenuation} = \frac{1}{f^2} \quad [3]$$

As the frequency of a particular transmission is increased, the level of attenuation of the signal in the ionosphere decreases. This means that a doubling of the frequency reduces the level of attenuation by a factor of four.

As the frequency is increased, the wavelength shortens, and collisions between free electrons and gas molecules decrease (i.e. there are fewer electrons per wavelength). Signals exceeding 30-35 MHz pass through the ionosphere into space (trans-ionospheric propagation) (19), (see discussion on the High Frequency (HF) band classification range discussion in Section J).

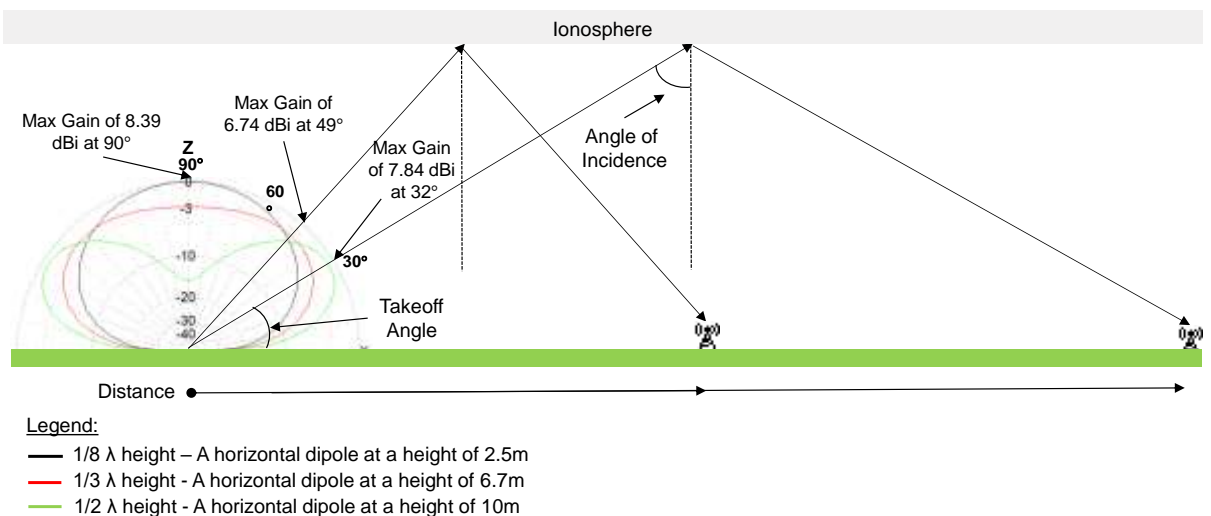
Generally, lower frequency transmissions are reflected by the lower layers of the ionosphere while the higher frequencies are reflected by the higher layers during the day.

Take-off Angles

Conceptually, when describing the take-off angle of a radio signal one thinks of a single ray travelling on a specific trajectory, while in practice take-off angles refers to the directionality and gain of an antenna. For the purposes of this analysis, a take-off (θ_t) angle of 90° is straight up, directly overhead, and at take-off angle of 0° is directed flat towards the horizon. Accordingly, the angle of incidence is referenced with respect to a perpendicular line such that the angle of incidence (θ_i) = $90^\circ - (\theta_t)$. Therefore, a take-off angle of 90° yields a 0° angle of incidence.

The illustration below demonstrates the relationship between skip distance and take-off angles. As a rule of thumb, the lower the take-off angle a signal is, further it goes. The illustration below includes the far field charts (created in the antenna modelling software MMANA-GAL) which compare the field strength, expressed in dBi, of a signal at some distant point relative to an isotropic antenna (a purely theoretical and omnidirectional antenna in free space).

Figure 6: Illustrative take-off angles & angles of incidence



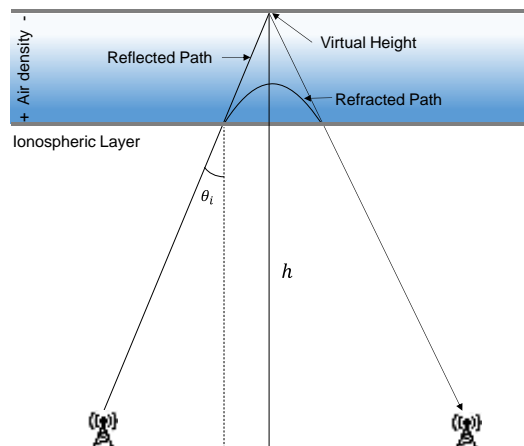
Source: W3LLA, far field charts generated using MMANA-Gal Software for a 20M center-fed dipole

C. Virtual Height

As a signal ascends towards the ionosphere, the particle density of the atmosphere it travels through decreases. This means that the signal travels from a dense medium to a thinner medium, and therefore the signal will refract when it enters the ionosphere provided that the angle of incidence (θ_i) is greater than the critical angle of 0° (a 90° trajectory straight up from the point of transmission).

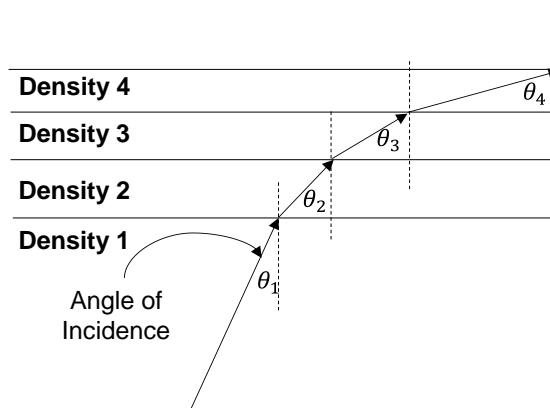
In a simplistic model, it is conceptualized that a signal reflects off of the ionosphere at a particular height without regard to the process of refraction taking place. The height at which the signal changes direction is considered to be the “virtual height”, and this height is used in geometric models to determine skip distances (3).

Figure 7: Virtual height



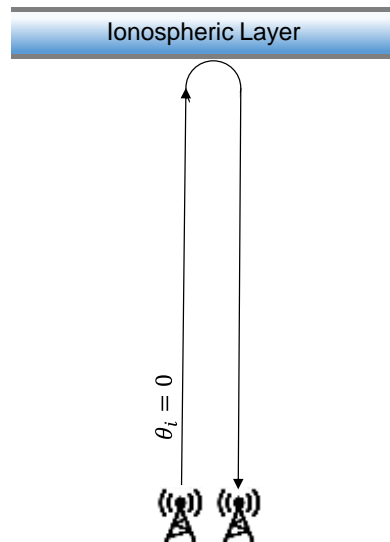
Because the changes in the air density are gradual, the process of refraction is also gradual, and the signal undergoes a constant process of refraction until the point where the signal is bent back and travels back towards the Earth. The signal is refracted back when the angle of incidence $\theta_i = \pi/2$, or 90° (3).

Figure 8: Layered Conceptualization of the Ionosphere (3; 20)



In practice, the virtual height is measured by an instrument called an ionosonde. An ionosonde transmits a signal vertically upward in pulses of different frequencies. Essentially, the ionosonde sweeps the HF spectrum transmitting at increasingly higher frequencies until the point where a return signal is no longer registered, effectively determining the maximum frequency for propagation directly overhead. The receiving station for these pulses is placed next to the transmitting station, and the virtual height can be determined using the time difference of arrival of the signal.

Figure 9: Vertical incidence



Using the formula:

$$Distance = velocity \times time (t)$$

One can assume that distance of travel is twice the height while the velocity is the speed of light (c). Therefore, the virtual height (h) can be determined to be:

$$2h = c \times t$$

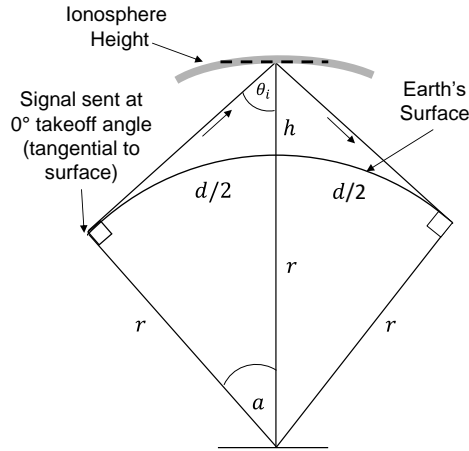
Thus:

$$h = \frac{1}{2}c \times t \quad [4]$$

D. Take-off Angles and the Ionization Layers – A Simplified Model

In a Simplified Model (21), if one assumes a signal is sent at a zero degree take-off angle to the Earth, a line tangential to the Earth is formed. This allows one to estimate the maximum distance a signal can travel in one hop if the height of the ionospheric refraction is known.

Figure 10: Simplified geometric ionospheric model



Ionosphere Height (km)	Single Skip Distance(km)
75	1,946
100	2,243
150	2,738
200	3,152
300	3,836
400	4,402

To measure the skip distance, on a curved Earth model, one can use the following:

$$\cos a = \frac{r}{r+h} = \frac{6,371\text{km}}{6,371\text{km} + 75\text{km}} = 0.9884 \quad [5]$$

$$\cos^{-1} a = 8.75^\circ = 0.1527 \text{ rad} \quad [6]$$

$$d/2 = r \times a \text{ rad} = 6,371\text{km} \times 0.1527 \text{ rad} = 973\text{km} \quad [7]$$

$$\therefore \text{total distance} = 2d = 1,946\text{km} \quad [8]$$

Where:

r = Volumetric mean radius of Earth $\cong 6,371\text{km}$ (NASA)

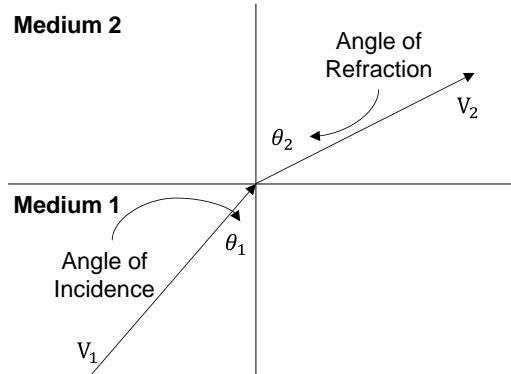
h = Assumed virtual height of the ionospheric reflection = 75km

Ionospheric refraction at the lower D layer of approximately 75km produces a single skip distance of approximately 2,000km while upper F Layer refraction generates distances of approximately 4,402km. The lower the take-off angle and higher the refraction height, the greatest single hop distance.

E. Snell's Law of Refraction

Snell's Law of Refraction describes a relationship of the angles of incidence and angles of refraction in reference to the speed of light traveling between different mediums.

Figure 11: Angles of incidence and refraction



In particular, Snell's Law explains that the ratio of velocity of light in medium two (V_2) to the sine of the angle of refraction (θ_2) equals the ratio of the velocity of light in medium one (V_1) to the sine of the angle of incidence (θ_1), (20):

$$\frac{V_2}{\sin \theta_2} = \frac{V_1}{\sin \theta_1} \quad [9]$$

In this equation, Snell's Law is expressed in velocity (V) but it can also be expressed as an index of refraction (n), which is the ratio of the speed of light in a vacuum to that of the speed of light in a second medium of higher density (20).

$$n = \frac{c}{v} \quad [10]$$

Where:

$$\text{Index of refraction} = \frac{\text{Speed of light in a vacuum}}{\text{Speed of light in the second medium}}$$

Thus, expressing in terms of velocity:

$$v = \frac{c}{n} \quad [11]$$

Therefore, for Medium 2:

$$\frac{V_2}{\sin \theta_2} = \frac{c}{n_2 \sin \theta_2} \quad [12]$$

Therefore Snell's Law expressed in terms of the refractive index is as follows:

$$\frac{\frac{c}{n_2}}{\sin \theta_2} = \frac{\frac{c}{n_1}}{\sin \theta_1} \quad [13]$$

By cross-multiplying, this equation can be converted to:

$$\sin \theta_2 \frac{c}{n_1} = \sin \theta_1 \frac{c}{n_2} \quad [14]$$

This can be written as:

$$\frac{\sin \theta_2 c}{n_1} = \frac{\sin \theta_1 c}{n_2} \quad [15]$$

By cross-multiplying again, this equation can be converted to:

$$n_2 \sin \theta_2 c = n_1 \sin \theta_1 c \quad [16]$$

Snell's Law can therefore be restated as follows:

$$n_2 \sin \theta_2 = n_1 \sin \theta_1 \quad [17]$$

where the index of refraction (n_2) for the second medium times the sine of the angle of refraction equals the refraction index for the first medium times the sine of the angle of incidence.

Therefore:

$$\frac{n_2 \sin \theta_2}{n_1} = \frac{n_1 \sin \theta_1}{n_1} \quad [18]$$

This can be expressed as:

$$\frac{n_2}{n_1} \sin \theta_2 = \sin \theta_1 \quad [19]$$

And:

$$\frac{n_2}{n_1} = \frac{\sin \theta_1}{\sin \theta_2} \quad [20]$$

Therefore, expressing Snell's Law in terms of velocity from Equation [9]:

$$\frac{V_2}{\sin \theta_2} = \frac{V_1}{\sin \theta_1}$$

Equates to:

$$\frac{V_1}{V_2} = \frac{\sin \theta_1}{\sin \theta_2} = \frac{n_2}{n_1} \quad [21]$$

F. Critical Frequency

At any given point in time within each layer of the ionosphere, there is maximum frequency where a radio signal, if transmitted into it vertically, will be reflected back to Earth. (12) This frequency is called the Critical Frequency (f_c) or the plasma frequency. The refraction index of the ionosphere can be used to determine the Critical Frequency. The refraction index of the ionosphere (n) is defined as (22):

$$n = \sqrt{1 - \frac{81N}{f^2}} \quad [22]$$

where N is the number density of electrons (electron density) per cubic meter. From the above equation one can see that the refraction index for the ionosphere is a function of the electron density.

The plasma critical frequency is also directly proportional (\propto) to the (negatively charged e^-) electron density times a constant K (19):

$$f_c \propto [e^-] \times K \quad [23]$$

Equation [21] of Snell's Law states:

$$\frac{V_1}{V_2} = \frac{\sin \theta_1}{\sin \theta_2} = \frac{n_2}{n_1}$$

where n_2 is the index of refraction for the ionosphere in relation to n_1 , and where n_1 is indexed to 1, which makes the ratio of n_2 to n_1 equal to n_2 or simply "n".

Therefore, for a frequency which equals the critical frequency ($f = f_c$) and for an angle of incidence θ_1 , the critical frequency is calculated as follows:

$$\frac{\sin \theta_1}{\sin \theta_2} = \sqrt{1 - \frac{81N}{f^2}} \quad [24]$$

For a critical frequency f_c , the angle of incidence is $\theta_1 = 0 \text{ degrees}$, and since $\sin 0^\circ = 0$, this equation can be converted to:

$$0 = \sqrt{1 - \frac{81N}{f^2}} \quad [25]$$

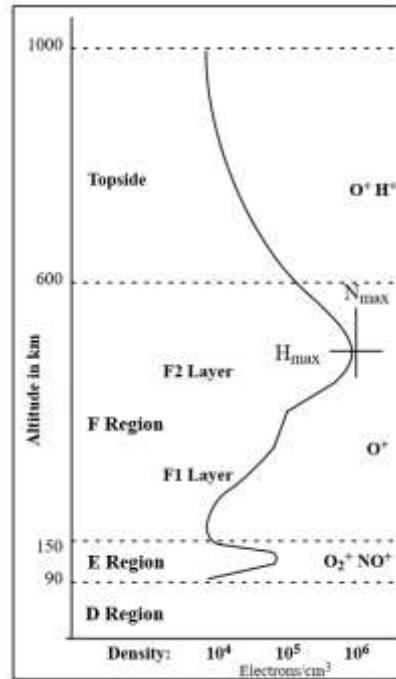
$$\frac{81N}{f^2} = 1 \quad [26]$$

$$f_c = \sqrt{81N} = 9\sqrt{N} \quad [27]$$

where N is maximum electron density per m^3 and f_c is expressed in Hz.

This means that the critical frequency can be calculated directly from the electron density of any particular layer.

Figure 12: Illustrative ionosphere electron density profile



Source: NOAA, Reproduced from Anderson and Fuller-Rowell (1999).

At higher altitudes, the variability in electron density is substantial. By way of approximation, converting the electron density N to a critical frequency by ionosphere layer using Figure 12 data, the following calculations can be made:

$$D \text{ Layer } f_c = 9\sqrt{N} = 9\sqrt{10^4} = 900 \text{ Hz}$$

$$E \text{ Layer } f_c = 9\sqrt{N} = 9\sqrt{10^5} = 2.8 \text{ MHz}$$

$$F \text{ Layer } f_c = 9\sqrt{N} = 9\sqrt{10^6} = 9.0 \text{ MHz}$$

From this one can see that in order to have a signal reach the F Layers, it needs to pass through the lower D and E layers, and thus require higher frequencies.

G. Maximum Usable Frequency

The Maximum Usable Frequency (MuF) is defined as the highest frequency that can be used between two points on Earth using sky wave, ionospheric propagation. In practice the MuF can be determined by steadily increasing the frequency in a communication circuit until the point where the receiving station can no longer hear the signal.

Similar to the Critical Frequency, the MuF has a mathematical relation to the index of refraction for the ionosphere and Snell's Law (3; 4).

MuF relates to signals that enter the ionosphere obliquely rather than vertically as in the case of critical frequency. As a result, the angle of incidence θ_1 is greater than 0° and the most that the angle of reflection θ_2 could be is 90° , which would represent the maximum angle of incidence.

For a frequency which equals the maximum usable frequency, where $f = f_{muf}$, and the angle of incidence θ_1 is assumed to be $0^\circ > \theta_1 \leq 90^\circ$, Maximum Usable Frequency is calculated as follows:

$$\frac{\sin \theta_1}{\sin \theta_2} = \sqrt{1 - \frac{81N}{f^2}} \quad [28]$$

Since the maximum angle of reflection θ_2 is 90° , and $\sin 90^\circ = 1$, MuF can be calculated:

$$\frac{\sin \theta_1}{\sin 90^\circ} = \sqrt{1 - \frac{81N}{f^2}} \quad [29]$$

$$\sin^2 \theta_1 = 1 - \frac{81N}{f^2} \quad [30]$$

$$\frac{81N}{f^2} = 1 - \sin^2 \theta_1 \quad [31]$$

Using Pythagorean's trigonometric identity, it can be restated:

$$\frac{81N}{f^2} = \cos^2 \theta_1 \quad [32]$$

$$\frac{81N}{\cos^2 \theta_1} = f^2 \quad [33]$$

$$\sqrt{\frac{81N}{\cos^2 \theta_1}} = f \quad [34]$$

Therefore:

$$\frac{9\sqrt{N}}{\cos\theta_1} = f = MuF \quad [35]$$

Using a reciprocal trigonometric identity ($\sec\theta_1 = \frac{1}{\cos\theta_1}$) and substituting in the equation for Critical Frequency f_c (Equation 27), one can relate vertical to oblique-incident transmissions (23):

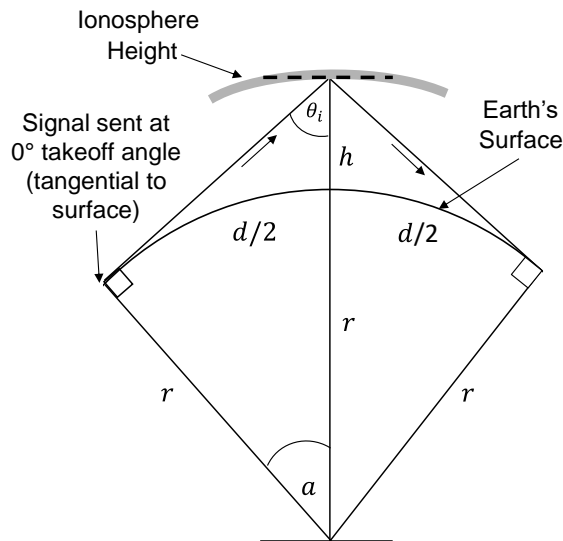
$$MuF = f_c \sec\theta_1 \quad [36]$$

H. Expanded Model

The Simplified Model described in Section D dealt with signals directed at a zero degree take-off angle to the Earth and estimated a geometric maximum distance a signal can travel in one hop based on an assumed height of the ionospheric refraction. In this analysis, the Simplified Model is expanded by considering the angle of incidence together with the formulas for Critical Frequency and Maximum Usable Frequency.

In this model, a virtual height is assumed to be 300km (a mid-range F region altitude), and a volumetric mean radius of the Earth is assumed to be 6,371km. Using these parameters, the calculations below determine a skip distance of 3,837km and a maximum θ_i of approximately 73°:

Figure 13: Expanded ionospheric model



Measuring the curvature of the Earth as to determine skip distance we have the following:

$$\cos a = \frac{r}{r + h} = \frac{6,371\text{km}}{6,371\text{km} + 300\text{km}} = 0.9550 \quad [37]$$

$$\cos^{-1} a = 17.25^\circ = 0.3011 \text{ rad} \quad [38]$$

$$d/2 = r \times a \text{ rad} = 6,371\text{km} \times 0.3011 \text{ rad} = 1,919\text{km} \quad [39]$$

$$\therefore \text{total distance} = 2d = 3,837\text{km} \quad [40]$$

Therefore, the angle of incidence θ_i is:

$$\sin \theta_i = \frac{r}{r+h} = \frac{6,371km}{6,371km + 300km} = 0.9550 \quad [41]$$

$$\sin^{-1} \theta_i = 72.75^\circ \quad [42]$$

Once a height is determined and the angle of incidence θ_i is calculated, a determination is then made as to the electron density at that particular altitude. In this example, an electron density of $10^{4.8}$ electrons/cm³ was chosen for purely illustrative purposes (refer to the Amended NOAA Electron Density Profile (9)). From this one can determine the corresponding MuF, and Critical Frequency f_c relating to transmissions with the corresponding virtual height and electron density parameters. From equation [36] one can solve for MuF.

$$MuF = \frac{9\sqrt{N}}{\cos\theta_i}, \text{ where } 9\sqrt{N} \text{ is the } f_c, \text{ thus:} \quad [43]$$

$$MuF = 7,624Hz = \frac{9\sqrt{10^{4.8}}}{\cos 72.75^\circ}, \text{ where } f_c = 2,261Hz \quad [44]$$

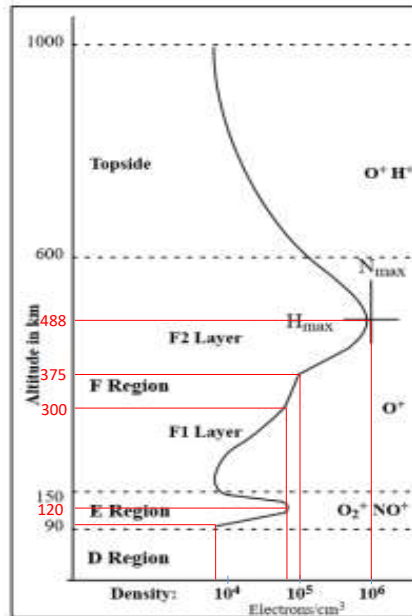
Where:

r = Volumetric mean radius of Earth $\cong 6,371km$ (NASA)

h = Assumed virtual height of the ionospheric reflection = 300km

N = Maximum electron density (electrons/cm³) at the virtual height (h) = $10^{4.8}$

Figure 14: Amended NOAA electron density profile



Source: NOAA with approximated overlay by W3LLA (in red)

The electron density profile from Figure 14 represents a normalized and static depiction of electron counts at altitude and is an amalgamation of solar maximum and minimum, and daytime and night time electron counts (as evidenced by the whipsawing of the density between regions). Electron density profiles as shown in Figure 18 on page 35 depicts a normalized electron density profile with the diurnal influences separated.

Though limited in practical usefulness, Figure 14 is instructive in providing a relative sense of the interplay between MuF, critical frequency and skip distance with electron density and virtual height when it is incorporated to an expanded model. From the approximated benchmark altitudes and electron counts which overly the chart (in red), the corresponding figures for MuF, Critical Frequency, angles of incidence are derived.

Table 1: Expanded Model - 0° take-off angle¹

0° Degree Take-off Angle - Expanded									
Virtual Height (km)	Electron Density (per cm ³)	N (per cm ³)	sin θ_i	θ_i °	cos θ_i	f_c (Hz)	MuF (Hz)	λ (m)	Skip Distance (km)
90	10 ^{3.75}	5,623	0.9861	80.4	0.1663	675	4,058	74	2,129
120	10 ^{4.8}	63,096	0.9815	79.0	0.1914	2,261	11,812	25	2,454
300	10 ^{4.8}	63,096	0.9550	72.8	0.2965	2,261	7,624	39	3,836
375	10 ⁵	100,000	0.9444	70.8	0.3288	2,846	8,657	35	4,269
488	10 ⁶	1,000,000	0.9289	68.3	0.3704	9,000	24,295	12	4,835

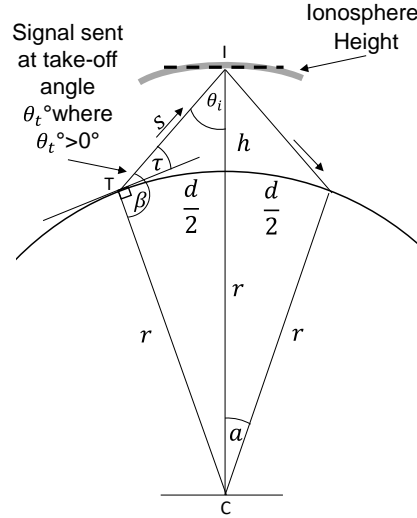
Source: W3LLA

The table above shows calculations of MuF based on the electron density relative to the virtual height, take-off angle, and therefore distance. They illustrate the key considerations (or limitations) that a radio operator must contend with when choosing a frequency for a desired distance.

Central to the analysis in Table 1 is the assumption that the signals are sent at a perfect grazing angle to the Earth, i.e. a zero degree take-off angle. Because in practice this is impracticable, take-off angles exceeding 0° would likely be used instead. To determine the skip distance of the arc of the curve of the Earth's radius, the expanded model incorporates the use of the Law of Sines to determine the relevant angle of incidence for the transmission.

¹ The figures for electron density are approximated from the NOAA Electron Density Profile in Figure 14: Amended NOAA electron density profile and are for purely illustrative purposes.

Figure 15: Expanded ionospheric model with take-off angles $>0^\circ$



Assuming a take-off angle τ of 30° , β will thus equal 90° plus τ , or 120° . Using the Law of Sines for ΔTIC :

$$\frac{\sin \theta_i}{r} = \frac{\sin \beta}{r+h} = \frac{\sin \theta_a}{s} \quad [45]$$

Focusing on the first two expressions:

$$\frac{\sin \theta_i}{r} = \frac{\sin \beta}{r+h} \quad [46]$$

Thus:

$$\frac{\sin \theta_i}{6,371km} = \frac{\sin 120^\circ}{6,371km + 300km}$$

Where:

$r =$ the volumetric mean radius of the earth $\cong 6,371km$

$h =$ the assumed virtual height of the ionospheric refraction = $300km$

Therefore:

$$\sin \theta_i = \frac{6,371km \sin 120^\circ}{6,371km + 300km} = 0.8271 \quad [47]$$

$$\sin^{-1} \theta_i = 55.8^\circ \quad [48]$$

Solving for angle a :

$$180^\circ - \theta_i - \beta = a = 180^\circ - 55.8^\circ - 120^\circ = 4.2^\circ \quad [49]$$

Thus, skip distance d is calculated as follows:

$$\frac{d}{2} = \left(4.2^\circ \frac{\pi}{180}\right) \times r = 0.0733 \times 6,371km = 467km \quad [50]$$

Thus:

$$d = 2 \times 467km = 934km \quad [51]$$

Adjusting the analysis found in Table 1 for a higher take-off angle of 30° yields the following:

Table 2: Expanded Model - 30° take-off angle¹

30° Degree Take-off Angle - Expanded									
Virtual Height (km)	Electron Density (per cm ³)	N (per cm ³)	sin θ_i	θ_i °	cos θ_i	f_c (Hz)	MuF (Hz)	λ (m)	Skip Distance (km)
90	10 ^{3.75}	5,623	0.8540	58.6	0.5203	675	1,297	231	301
120	10 ^{4.8}	63,096	0.8500	58.2	0.5268	2,261	4,292	70	397
300	10 ^{4.8}	63,096	0.8271	55.8	0.5621	2,261	4,022	75	934
375	10 ⁵	100,000	0.8179	54.9	0.5754	2,846	4,946	61	1,140
488	10 ⁶	1,000,000	0.8044	53.6	0.5941	9,000	15,150	20	1,434

Interestingly, the table shows a dramatic change in skip distances and MuF in response to a change in take-off angles.

Assuming the electron density profile at various heights detailed above, the relevant signal and skip characteristics at various take-off angles are then calculated (below). As the take-off angle approaches 90° (directly overhead), the angle of incidence to the ionosphere approaches 0° and thus the MuF converges with the critical frequency while skip distances reduce to zero. From this the frequency impact of a vertical incidence signal versus oblique incidence can be seen where increasingly oblique signals are able to accommodate increasingly higher frequency signals and as take-off angles approach 90°, MuF approaches critical frequency.

Table 3: Expanded Model – propagation matrix

Take-off Angle	90km Virtual Height			Take-off Angle	300km Virtual Height			Take-off Angle	488km Virtual Height		
	fc(Hz)	MuF(Hz)	Skip Distance (km)		fc(Hz)	MuF(Hz)	Skip Distance (km)		fc(Hz)	MuF(Hz)	Skip Distance (km)
0°	675	4,058	2,129	0°	2261	7,624	3,836	0°	9000	24,295	4,836
5°	675	3,605	1,288	5°	2261	7,341	2,877	5°	9000	23,735	3,844
10°	675	2,827	848	10°	2261	6,654	2,193	10°	9000	22,275	3,076
15°	675	2,215	608	15°	2261	5,856	1,714	15°	9000	20,380	2,492
20°	675	1,795	465	20°	2261	5,125	1,374	20°	9000	18,442	2,048
25°	675	1,504	369	25°	2261	4,514	1,124	25°	9000	16,674	1,705
30°	675	1,297	301	30°	2261	4,022	934	30°	9000	15,150	1,434
35°	675	1,145	250	35°	2261	3,629	784	35°	9000	13,870	1,214
40°	675	1,030	210	40°	2261	3,316	663	40°	9000	12,809	1,032
45°	675	942	176	45°	2261	3,065	561	45°	9000	11,935	877
50°	675	873	148	50°	2261	2,864	474	50°	9000	11,219	743
55°	675	818	124	55°	2261	2,702	397	55°	9000	10,635	624
60°	675	776	102	60°	2261	2,573	328	60°	9000	10,162	518
65°	675	742	83	65°	2261	2,471	266	65°	9000	9,785	420
70°	675	717	65	70°	2261	2,392	208	70°	9000	9,492	329
75°	675	698	48	75°	2261	2,333	153	75°	9000	9,272	242
80°	675	685	31	80°	2261	2,292	101	80°	9000	9,119	160
85°	675	677	16	85°	2261	2,269	50	85°	9000	9,030	79
90°	675	675	-	90°	2261	2,261	-	90°	9000	9,000	-

¹ The figures for electron density are approximated from the NOAA Electron Density Profile and are for purely illustrative purposes

I. Effective Earth Radius and Skip Distance

The Simplistic and Expanded Models described in Sections D and H deal with skip distance in relation to: take-off angle, angle of incidence, and an assumed virtual height of signal reflection. These sections demonstrate the relationship between the refractive index of the ionosphere, electron density, and signal frequency.

In these geometric models, an assumed virtual height, take-off angle, and Earth radius determine skip distance trigonometrically. Furthermore, an implied critical frequency and maximum usable frequency are derived from an assumed electron density at a given elevation and from the index of refraction Equation [22] for the ionosphere.

As illustrated in Figure 3 and Figure 8, the air density of the atmosphere decreases with altitude in normal conditions. As a radio signal ascends into the ionosphere, it enters a medium whose index of refraction gradually decreases with altitude. As a result, the signal travels at a higher velocity in a less dense medium at higher altitudes relative to traveling at a lower velocity in the denser medium closer to the Earth's surface (24). This vertical velocity differential and change in the index of refraction gives rise to signal refraction as the signal bends downwards towards the slower, denser medium, returning back to Earth (25). This refraction has the effect of extending the radio horizon beyond the visible or geometric horizon, and as a result skip distances will be longer than those presented in purely geometric models.

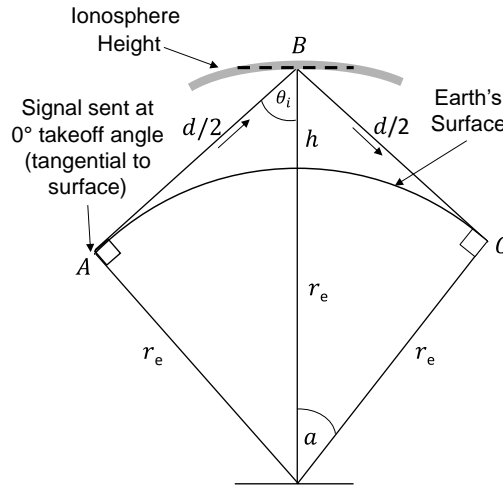
Conceptually, if it assumed that the index of refraction decreases in a uniform and linear fashion, it can also be assumed that the rate of “bending” of the signal will also be uniform. Therefore, this uniform refraction for the signal can be represented as a straight-line, provided that it is assumed that the radius of the Earth is adjusted in a way that the curve of the straight line signal maintains its proportions relative to the radius of the Earth. This is accomplished by changing the radius of the Earth by a scale factor “K” (24; 25; 26). If the proper scale factor is applied, the straight line distances of the signal rays will be identical to curved path distances.

For typical refraction conditions with a consistent vertical refraction gradient, (r_e) is determined to be:

$$r_e = r \left(\frac{4}{3} \right) \quad [52]$$

Where r is the volumetric mean radius of 6,371km multiplied by a scale factor of 1.33 which yields an effective Earth radius of 8,495km (27; 26) compared to the volumetric mean radius of 6,371km.

Figure 16: Straight path maximum distance using r_e with a 0° take-off angle



As a rule of thumb, maximum distance can be reduced to a simple approximated equation by using the straight signal path line distance rather than the curved surface of the Earth if an effective Earth radius is used (22; 3). In the above figure this “straight line path” is the distance ABC . Using Pythagorean’s Theorem:

$$\left(\frac{d}{2}\right)^2 = (r_e + h)^2 - r_e^2 \quad [53]$$

$$\left(\frac{d}{2}\right)^2 = r_e^2 + 2r_e h + h^2 - r_e^2 \quad [54]$$

$$\left(\frac{d}{2}\right)^2 = 2r_e h + h^2 \quad [55]$$

$$\frac{d}{2} = \sqrt{2r_e h + h^2} \quad [56]$$

$$d = 2\sqrt{2r_e h + h^2} \quad [57]$$

Using an effective earth radius of 8,495km and assuming a virtual ionospheric reflection height of 300km, a maximum skip distance would be calculated as:

$$d = 2\sqrt{2 \times 8,495\text{km} \times 300\text{km} + (300\text{km})^2} \quad [58]$$

$$d = 4,555\text{km} \quad [59]$$

The straight signal path line distance rather than the curved surface of the Earth using an effective Earth radius we have:

$$\left(\frac{d}{2}\right)^2 = h(2r_e + h) \quad [60]$$

Since the diameter of the Earth expressed as $2r_e$ is much larger than h , the expression $(2r_e + h)$ can be replaced by simply using $2r_e$, and the resulting error will be minimal (<http://www.phy6.org/stargaze/Shorizon.htm>). As a result, the maximum skip distance can be calculated as follows:

$$\left(\frac{d}{2}\right)^2 = 2hr_e \quad [61]$$

$$\frac{d}{2} = \sqrt{2hr_e} \quad [62]$$

$$d = 2\sqrt{2hr_e} \quad [63]$$

This gives:

$$d = 2\sqrt{2 \times 8,495km \times 300km} = 4,515km \quad [64]$$

The resulting difference is a mere 40km, and therefore, for simplicity, Equation [63] is often used instead of Equation [57] to calculate the maximum skip distance.

J. Validating the Effective Earth Radius Using the Expanded Model

In the previous sections, the Expanded Model was used to determine Critical Frequencies and Maximum Usable Frequencies using the geometric Earth radius. This then allowed one to determine a basic profile for maximum theoretical single skip distance.

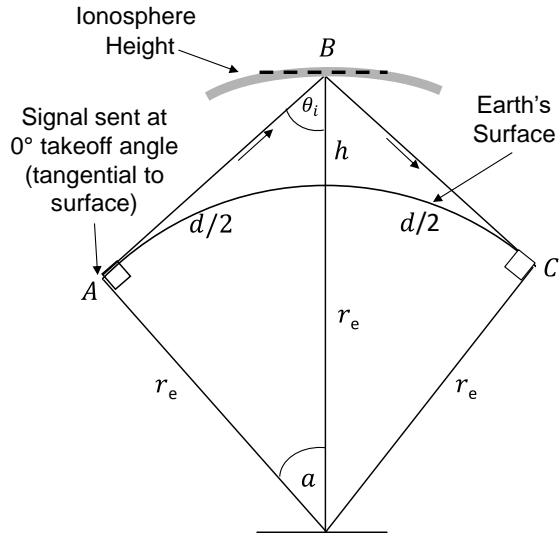
As demonstrated earlier, the maximum theoretical angle of incidence θ_i is a function of the altitude of ionospheric refraction and radius of the Earth, and it is maximized at a 0° take-off angle. Using a likely maximum virtual height of reflection at 300km (a mid-range F region altitude) and the geometric Earth radius of 6,371km yields a maximum angle of incidence (θ_i) of approximately 73° (see section H on the Expanded Model). Similarly, using the effective Earth radius of 8,495km yields a maximum angle of incidence of approximately 75° (Equation [66]), hence the 74° (average) rule of thumb is commonly referenced (3).

$$\sin \theta_i = \frac{r}{r + h} = \frac{8,495km}{8,495km + 300km} = 0.9659 \quad [65]$$

$$\sin^{-1} \theta_i = 74.99^\circ$$

[66]

Figure 17: Curved path maximum distance using r_e with a 0° take-off angle



Ionosphere Height (km)	Single Skip Distance(km)
75	2,249
100	2,594
150	3,170
200	3,651
300	4,450
400	5,114

In this section, instead of the straight line path, the curvature of the Earth will be measured to determine skip distances while using the effective Earth radius:

$$\cos a = \frac{r_e}{r_e + h} = \frac{8,495\text{km}}{8,495\text{km} + 300\text{km}} = 0.9659 \quad [67]$$

$$\cos^{-1} a = 15.01^\circ = 0.2619 \text{ rad} \quad [68]$$

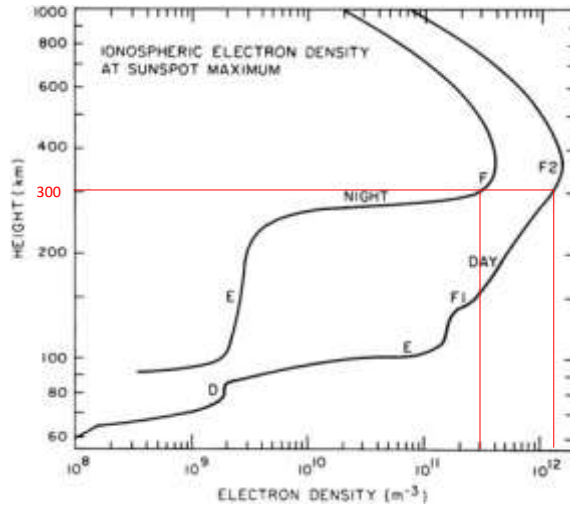
$$d/2 = r_e \times a \text{ rad} = 8,495\text{km} \times 0.2619 \text{ rad} = 2,225\text{km} \quad [69]$$

$$\therefore \text{total distance} = 2d = 4,450\text{km} \quad [70]$$

The total skip distance using this method detailed in Equation [70] validates the previous method detailed in Equation [64]: the difference is approximately 5 km. This confirms that despite the simplification introduced by using the straight line path, these prior models can still be used as a good “rule of thumb” to measure the total skip distance.

Fixing the assumption of virtual height at 300km (a typical mid-range F region altitude), an effective Earth radius of 8,495km, and a 0° take-off angle, one can determine the corresponding Maximum Usable Frequencies. Expanding upon the electron density profile from Figure 14, a “normalized” electron density is applied here which separates daytime and nighttime electron density curves during sunspot maximum. Though the electron profile used here is purely illustrative and static, it does provide a rough sense of the MuF and Critical Frequency under during typical solar maximum band conditions.

Figure 18: Ionospheric electron density at sunspot maximum - illustrative



Source: (28) with approximated overlay by W3LLA (in red)

An approximate range of electron density N of 10^{11} to 10^{12} (m^3) or 10^5 to 10^6 (cm^3) at a reflective altitude of 300km translates to MuF and critical frequency as follows:

$$MuF = \frac{9\sqrt{N}}{\cos\theta_i}, \text{ where } 9\sqrt{N} \text{ is the } f_c, \text{ thus:} \quad [71]$$

Where $N = 10^5 \text{ cm}^3$
Night Curve

$$MuF = 10,989\text{Hz} = \frac{9\sqrt{10^5}}{\cos 74.99^\circ}, \text{ where } f_c = 2,846\text{Hz} \quad [72]$$

Where $N = 10^6 \text{ cm}^3$
Day Curve

$$MuF = 34,751\text{Hz} = \frac{9\sqrt{10^6}}{\cos 74.99^\circ}, \text{ where } f_c = 9,000\text{Hz} \quad [73]$$

Where $\cos 74.99^\circ$ is derived from Equation [66].

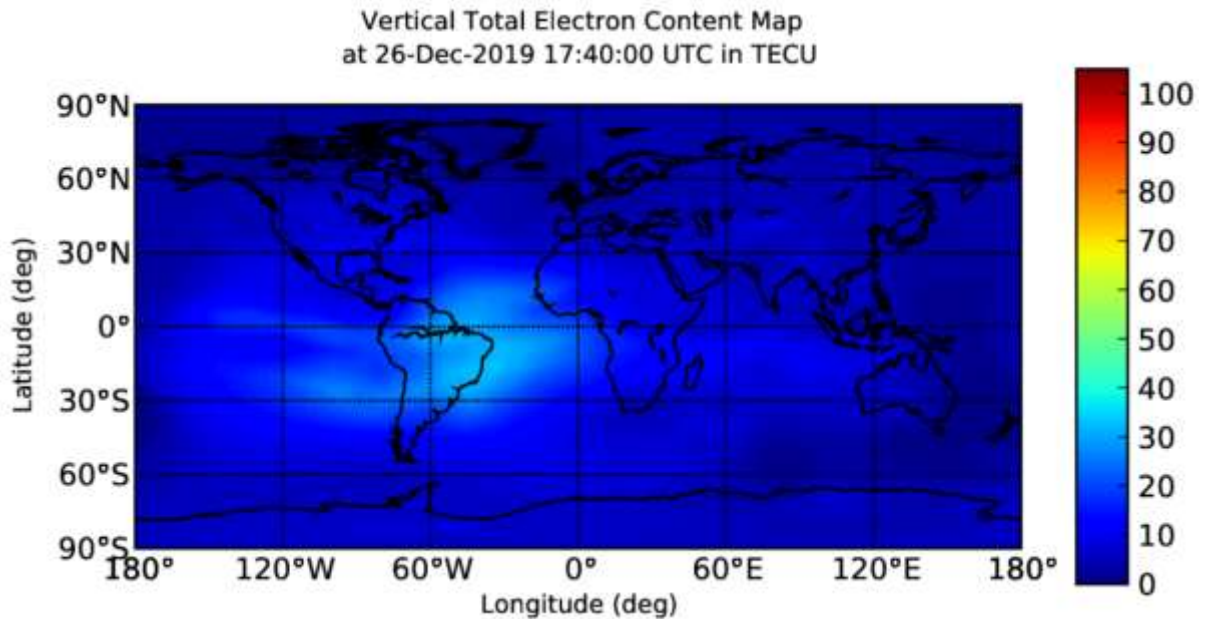
From this one can see the diurnal variations in critical frequency and MuF . Interestingly, the derived range in frequency from the f_c at night of 2.8MHz to the MuF of 34.8 MHz during the day under an idealized representation of electron count during solar maximum broadly reinforces the High Frequency (HF) band classification range of 3-30 MHz.

K. Ionosphere Tracking Models

In the prior sections, derived frequencies were based on a limited number of basic assumptions for electron counts at select altitudes which were derived from an approximated and “normalized” model of the ionosphere as seen in Figure 14. In practice however, electron counts at altitudes are extremely fluid and perpetually changing. Large variations in electron counts arise due to dynamics like diurnal changes in solar radiation, solar activity (e.g. flares), terrestrial weather, and the 11 year solar maximum and minimum. In fact, the amount of EUV and x-ray radiation varies by nearly a factor of ten over the 11 year solar cycle (29).

Having an understanding of electron counts in the ionosphere at various altitudes along a desired propagation path is helpful in determining frequency and take-off angles needed for a successful communications link. A number of public resources are available which seek to capture the current status of the ionosphere, and their output is generally distilled to a generalized characterization of “band conditions”. Below is an example of a real time map for total electron count (TEC) where 1 TEC Unit TECU = 10^{16} electrons/m² provided by NASA Jet Propulsion Laboratory.

Figure 19: Real time total electron count map

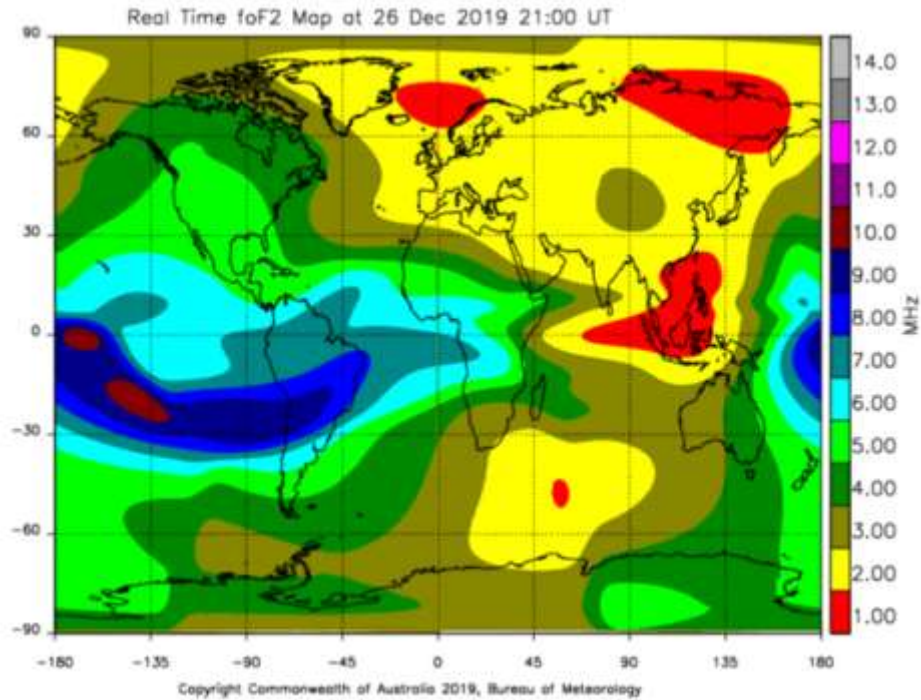


Another tool is the VOACAP HF Predictions tool. “VOACAP (Voice of America Coverage Analysis Program) is a free professional high-frequency (HF) propagation prediction software from NTIA/ITS, originally developed for Voice of America (VOA)”¹. The Australian Government Bureau of Meteorology

¹ <https://www.voacap.com/>

also provides a Space Weather Services tracking website which includes a worldwide, real time Critical Frequency heat map (Figure 20).

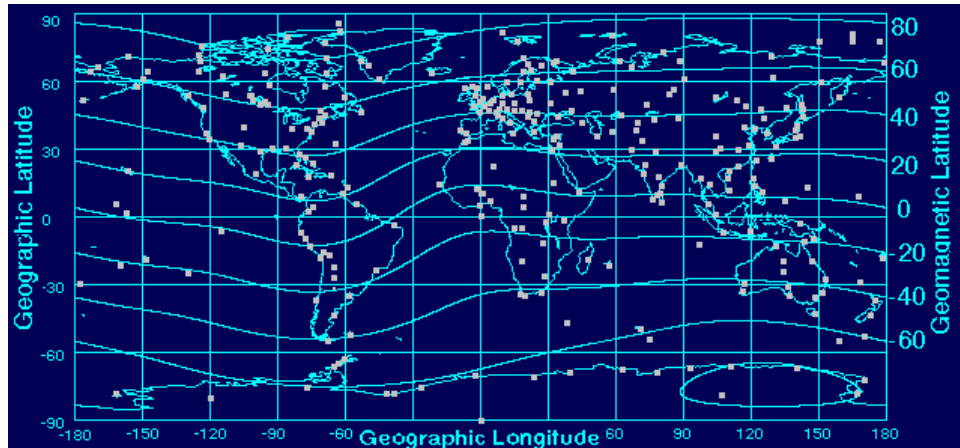
Figure 20: Real time foF2 (Critical Frequency)



https://www.sws.bom.gov.au/HF_Systems/6/5

The worldwide network of vertical incidence ionosondes is a widespread consortium network of ionosphere sensors which provide extremely detailed information for a discrete number of stations worldwide (30). Figure 21 demonstrates that while these ionosondes are spread over the Earth's surface, there remain large areas where the concentration of coverage is limited (e.g. oceans and deserts). Given the inconsistent concentration of ionosonde sensor points around the Earth, a large amount of extrapolation (and error) is imbedded into electron density coverage maps/models seeking to extrapolate ionospheric conditions from these sensor points.

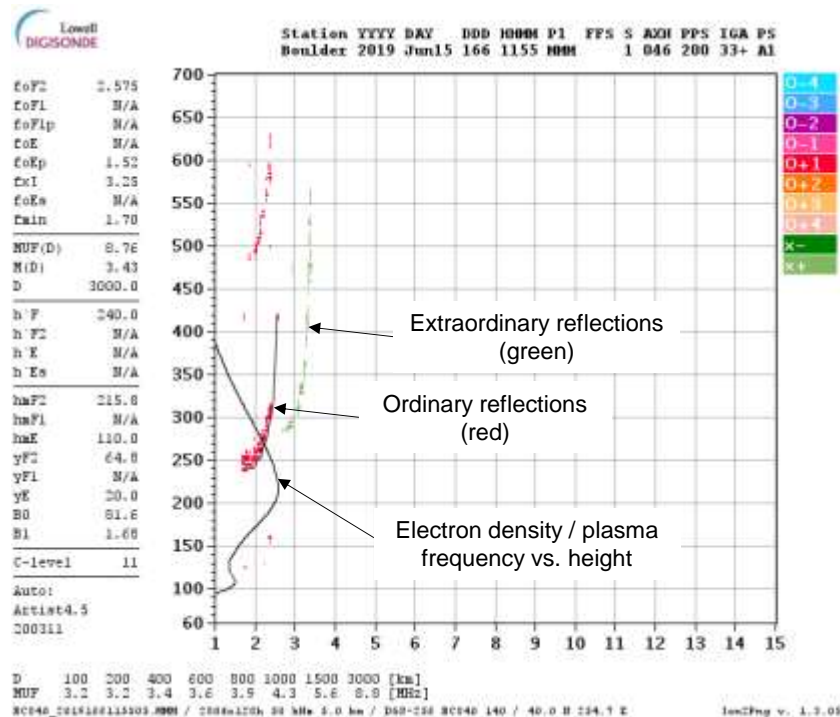
Figure 21: NOAA worldwide vertical ionosonde network – 130 Stations



Source: <https://www.ngdc.noaa.gov/stp/cdrom/ionocd.html>

Figure 22 below is an example of an ionogram produced by the NOAA ionosonde in Boulder, Colorado. This report was run at 11:55AM local time on June 15, 2019. The black line represents the electron density as plasma frequency against altitude. At this particular moment, the critical frequency (referred to as foF2) for Boulder Station was 2.575 MHz.

Figure 22: Illustrative ionogram report – June 15 2019



Source: <ftp://ftp.ngdc.noaa.gov/ionosonde/data/BC840/individual/2019/171/image/> with annotations by W3LLA

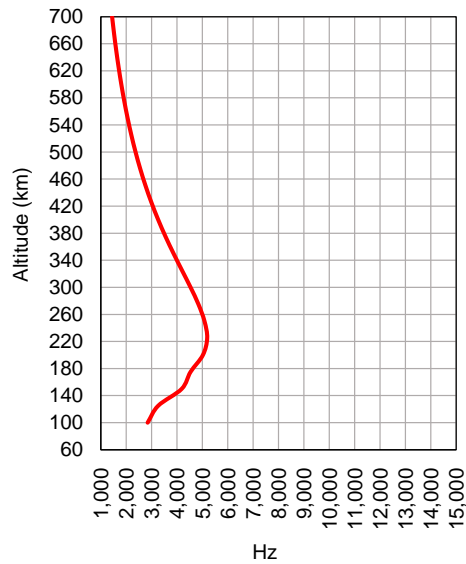
The International Reference Ionosonde (IRI) is an international ionosphere modelling project sponsored by the Committee on Space Research (COSPAR) and the International Union of Radio Science (URSI) to produce an “empirical standard model” of the ionosphere based on a number of data sources which

includes the global network of ionosondes, various radar installations, and measurements from various satellites. The IRI model provides public access to its data where, for any particular latitude and longitude and for any particular date and time, electron density at various altitudes can be obtained in customizable altitude increments from 65 to 2,000km. (31).

The IRI model, relying on a network of widespread sensor points, entails a high degree of extrapolation in order to model electron density profiles at any particular latitude and longitude. Ultimately, any derived report contains error, averaging, and approximation, and it should be viewed as indicative rather than definitive. By way of illustration, while an IRI report for electron density at altitude for the same latitude and longitude for the ionosonde at Boulder Station yielded a similar plasma frequency profile, the plasma/Critical Frequency was twice that of Boulder Station (see Figure 23). Most likely this discrepancy is due to the timing of the IRI run not coinciding with the precise timing of the Boulder probe. Moreover, the exact latitude and longitude of the IRI report may have been imprecise, and the IRI data itself is an extrapolated dataset, which would give rise to error.

Though not as accurate as an ionosonde, the IRI data can be instructive as it fills in the gaps geographically through extrapolation, and it provides another tool to monitor changes in electron densities.

Figure 23: Calculated Plasma Frequency – June 15 2019 Boulder Station using IRI Data

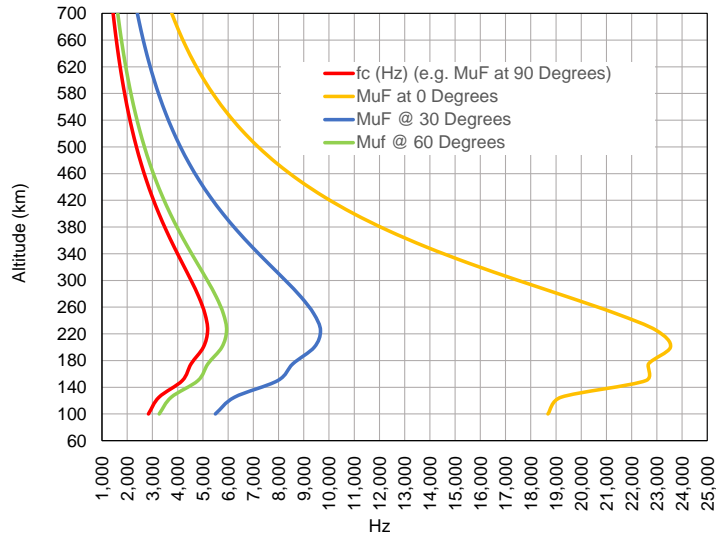


Source: W3LLA

Incorporating the IRI electron density information into the Expanded Model described in Section H yields more detailed, and perhaps more instructive calculations for Critical Frequency, Maximum Usable Frequency, and skip distance. When assessing a possible propagation path, one could use the IRI derived electron densities to determine a critical frequency for an assumed midpoint location between a transmitter and a receiver, and thus estimate a possible MuF between the locations. This

data can also be used retroactively to explain/illustrate a number of propagation/space weather characteristics.

Figure 24: Calculated plasma frequency & MuF at various take-off angles 6/15/19 Boulder Station using IRI data



Source: W3LLA

Table 4: Expanded Model using IRI electron density figures at Boulder Station (6/15/19)

0° Degree Take-off Angle - With Earth Radius Assumed to be 8495 km								Skip Distance (km)
Virtual Height (km)	N (cm ⁻³)	sin θ _i	θ _i °	cos θ _i	f _c (Hz)	MuF (Hz)	λ (m)	
100	99,674	0.9884	81.3	0.1521	2,841	18,681	16	2,594
125	131,020	0.9855	80.2	0.1697	3,258	19,198	16	2,897
150	216,260	0.9826	79.3	0.1855	4,185	22,565	13	3,170
175	253,560	0.9798	78.5	0.1999	4,532	22,670	13	3,419
200	311,040	0.9770	77.7	0.2133	5,019	23,537	13	3,651
225	332,220	0.9742	77.0	0.2257	5,187	22,984	13	3,868
250	318,740	0.9714	76.3	0.2374	5,081	21,403	14	4,072
275	289,510	0.9686	75.6	0.2485	4,843	19,490	15	4,266
300	253,630	0.9659	75.0	0.2590	4,533	17,503	17	4,450
325	217,370	0.9632	74.4	0.2690	4,196	15,601	19	4,626
350	184,140	0.9604	73.8	0.2785	3,862	13,866	22	4,795
375	155,250	0.9577	73.3	0.2877	3,546	12,326	24	4,958
400	130,890	0.9550	72.8	0.2965	3,256	10,981	27	5,114
425	110,670	0.9524	72.2	0.3050	2,994	9,817	31	5,266
450	94,010	0.9497	71.7	0.3132	2,759	8,811	34	5,412
475	80,315	0.9470	71.3	0.3211	2,551	7,943	38	5,554
500	69,043	0.9444	70.8	0.3288	2,365	7,193	42	5,691
525	59,736	0.9418	70.4	0.3362	2,200	6,543	46	5,825
550	52,015	0.9392	69.9	0.3434	2,053	5,977	50	5,955
575	45,577	0.9366	69.5	0.3504	1,921	5,483	55	6,082
600	40,177	0.9340	69.1	0.3572	1,804	5,050	59	6,206
625	35,623	0.9315	68.7	0.3638	1,699	4,669	64	6,326
650	31,758	0.9289	68.3	0.3703	1,604	4,332	69	6,444
675	28,460	0.9264	67.9	0.3766	1,518	4,032	74	6,559
700	25,630	0.9239	67.5	0.3827	1,441	3,765	80	6,672

III. Visualizing the Ionosphere Using the Weak Signal Propagation Reporter

A. Introduction

As described in the prior sections, long distance terrestrial radio communication using High Frequency (HF) radio signals in the range of 3-30 MHz depends upon the ionosphere, the electrically charged region of the upper atmosphere. HF radio signals are able to travel great distances due to a dynamic called Ionospheric Skip (a.k.a. sky wave) which entails radio waves “reflecting” off of the ionosphere to a distant point, often many thousands of kilometers from the originating station.

The formation of the ionosphere occurs in direct response to the impact of solar radiation on the upper regions of Earth’s atmosphere. The extreme solar energy, primarily EUV radiation and X -rays, strips atoms of their electrons creating ions and negatively charged electrons. These free electrons, whose concentration gradient changes with altitude, propagate radio signals and ultimately refract them back towards the Earth.

Because the ionosphere is an ever-changing and complex medium, HF sky wave communication remains unpredictable. At any particular moment in time, radio signals are either absorbed, refracted, or passed through the ionosphere. This depends on the signals’ wavelength and their angle of incidence as they enter the ionosphere in addition to the electron count of the ionosphere itself. If skip communication between two points is successful on any particular frequency for a desired distance, it is because ionospheric conditions permitted it; the frequency band is then deemed to be “open”.

Since the electron count in the ionosphere responds immediately to solar phenomena (e.g. solar flares, the 11 year sunspot cycle, and the diurnal effects of the Sun), it is reasonable to theorize that communication links using the ionosphere infer something about the state of the ionosphere, and that real time spot reports of successful communication links act as an indirect sensor and predictor of these phenomena.

Since its initial release in March 2008, radio operators have increasingly utilized the Weak Signal Propagation Reporter (WSPR), created by Dr. Joe Taylor, K1JT, Nobel Laureate (Physics, 1993) to test propagation paths mainly on the high frequency bands. WSPR is designed for sending and receiving low-power, narrow bandwidth, one-way, minimal information (call sign, location, & power level) transmissions in a reverse beacon format. Each WSPR transmission cycle starts on each even number minute and lasts approximately two minutes. At the end of each cycle, contact reports (“spots”) are automatically posted to the WSPR database. On any particular day, more than 2 million spots from

around the world are recorded; they represent a near real-time and large data-set which can be analysed.

The WSPR database posts in near-real time the successful communication links between a transmitting and receiving station for various frequencies. The WSPR reporters and transmitters in aggregate can be considered to be a large and distributed network of stations undertaking oblique soundings of the ionosphere at a point (or multiple points) along the path of the communication link.

In this demonstration experiment, it is anticipated that there would be some sort of relationship between spot reports and the time of day, and that spot reports (or lack thereof) would, in some way, track to the movement of the Sun. By using WSPR in a series of simple reverse beacon transmission experiments, it is possible to validate and visualize a number of the ionospheric dynamics:

- The impact on communication links when the transmission frequency is below or above the MUF
- The change in MUF (i.e. changes in the electron count in the ionosphere) in response to the diurnal effect of solar radiation by showing:
 - Propagation patterns in relation to the Sun's movement from east to west
 - Solar noon, count at day versus night when above the MUF
 - Reaction to sunrise and sunset
- The impact of the differing altitudes of the Ionospheric layers on skip distance by illustrating:
 - Daytime D Layer attenuation and impact on skip distance
 - Distance response to sunrise and sunset

B. Why WSPR? Narrow Bandwidth and Reduced Power: A Quick Primer

Communication using high frequency radio signals involves the use of many different modes, each using different techniques for modulating and encoding information to a radio wave. Broadly speaking, these modes can be divided into two major classifications: voice or digital. In voice communication, an audio signal is electronically added to (or mixed with) a carrier frequency and is then isolated at the receiving station where the audio signal can be understood. Amateur radio communications using voice is referred to as single sideband, or SSB, as the redundant/duplicated audio signal attached to a carrier frequency is eliminated to limit the signal's bandwidth. Nevertheless, SSB signals still require substantially more bandwidth than amateur digital modes. Typically, SSB transmissions require 2.4 to 3.0 kHz of bandwidth; this, in turn, brings an increase in signal noise which can be compensated for by using higher power transmissions (commonly up to 100 watts). SSB (voice) signals are limited by audio

voice filters in the transceiver which is around 2.4 to 3.0 kHz, a level which can handle the broader range of frequencies generated by the human voice and which is commonly recognized to be “an appropriate receive filter bandwidth to select in order to minimize noise and interference for SSB reception” (T4B09 ARRL Technician question pool, June 30 2018).

Conversely, narrow bandwidth or amateur digital modes require much less bandwidth because only a single tone (or a series of tones) is modulated. In the case of Morse Code (a.k.a. CW or Continuous Wave), a single, manually keyed tone generates the easily recognizable “dits and dahs”. Typical CW transmissions are only 100 Hz in bandwidth. For complex digital transmissions, like those sent using the Weak Signal Propagation Reporter (WSPR) mode, multiple tones are generated using a variable tone generator with the aid of a computer. Still, WSPR mode transmissions require bandwidth of only 6 Hz.

To emphasize: Voice communications using SSB have a bandwidth of 2,500Hz compared to 6Hz for WSPR mode.

The dramatic difference in bandwidths has an impact on the signal noise: the wide bandwidth signals have more signal noise to contend with compared to the more focused narrow bandwidth signals which have significantly less signal noise. This is analogous to the wide beam of a flashlight compared to a focused laser beam. To contend with this increase in noise, signal power is adjusted upward to increase a signal strength relative to the noise.

Comparing signal strength with the power level (watts) logarithmically, the relative strength of one signal vs. another is able to be determined and is referred to as “gain” which is expressed in decibels (db):

$$Gain (db) = 10 \times \log\left(\frac{P_2}{P_1}\right), \quad [74]$$

Where P_2 is the power setting in Watts of one transmission relative to a reference power level P_1 . For example, when comparing a SSB voice transmission of 100 watts relative to a typical QRP (reduced power) transmission of 5 Watts, a power ratio (multiple) of 20x, the following gain can be derived:

$$Gain (db) = 10 \times \log\left(\frac{100W}{5W}\right) = 13db \quad [75]$$

In amateur radio, signal strength is commonly referred to in signal units or “S” units where one S unit is equal to 6db of gain. A gain of 13db (or 20x) is approximately two S units.

To determine gain (or relative signal strength) of one particular mode versus another, the gain in power level should be considered in relation to the bandwidth of the particular modes being compared. To accomplish this, the gain of using one mode over another can be solved by comparing the power density (32) of each mode which is defined as:

$$\text{Power Density} = \frac{\text{Power (W)}}{\text{Bandwidth (Hz)}} \quad [76]$$

In the case of CW, where the typical bandwidth is 100 Hz, and SSB which uses a bandwidth of about 2,000 Hz, the power density for each transmission at 100 Watts would be calculated as

$$\text{Power Density CW} = \frac{100W}{100 \text{ Hz}} = 1 \text{ W/Hz} \quad [77]$$

$$\text{Power Density SSB} = \frac{100W}{2,000 \text{ Hz}} = 0.05 \text{ W/Hz} \quad [78]$$

Determining the decibel gain of using CW over SSB in terms of power density would then be calculated as:

$$\text{Gain (db)} = 10 \times \log\left(\frac{1}{0.05}\right) = 13\text{db} \quad [79]$$

Therefore, it can be stated that the gain of using CW over SSB voice would be 13db or 20x.

For an equivalent power level between the two modes, the power density of CW is equated to the power density of SSB. The equivalent power level (X) of CW can be determined where:

$$\frac{X}{100 \text{ (Hz)}} = \frac{100 \text{ (W)}}{2,000 \text{ (Hz)}} \quad [80]$$

$$\frac{X}{100 \text{ (Hz)}} = \frac{1 \text{ (W)}}{20 \text{ (Hz)}} \quad [81]$$

$$X = \frac{1 \text{ (W)}}{20 \text{ (Hz)}} \times 100 \text{ (Hz)} \quad [82]$$

$$X = 5W \quad [83]$$

Where X= the power level of CW (Watts).

This implies that using 5 Watts of power on CW is equivalent in signal strength to using 100 Watts for SSB voice transmission.

Taking this dynamic to the extreme, one can compare a typical SSB transmission (using 2,000 Hz) to a WSPR transmission which has a bandwidth of only 6 Hz. In order to determine an equivalent power level between the two, the power density of WSPR is equated to the power density of SSB. As result, the equivalent power level (X) of WSPR can be solved as follows:

$$\frac{X}{6 \text{ (Hz)}} = \frac{100 \text{ (W)}}{2,000 \text{ (Hz)}} \quad [84]$$

$$\frac{X}{6 \text{ (Hz)}} = \frac{1 \text{ (W)}}{20 \text{ (Hz)}} \quad [85]$$

$$X = \frac{1 \text{ (W)}}{20 \text{ (Hz)}} \times 6 \text{ (Hz)} \quad [86]$$

$$X = 0.3 \text{ W} \quad [87]$$

Where X= the power level of WSPR (Watts).

This means that using 0.3 Watts of power on WSPR is equivalent in signal strength to using 100 Watts for SSB voice transmission.

Using the power density of WSPR mode transmissions at 100 Watts calculated as follows:

$$\text{Power Density WSPR} = \frac{100\text{W}}{6 \text{ Hz}} = 16.67 \text{ W/Hz} \quad [88]$$

we can then calculate the decibel gain of a WSPR transmission over SSB as:

$$\text{Gain (db)} = 10 \times \log\left(\frac{16.67}{0.05}\right) = 25.2 \text{ db} \quad [89]$$

Therefore, it can be stated that the gain of using WSPR over SSB voice would be 25.2db or 333.3x.

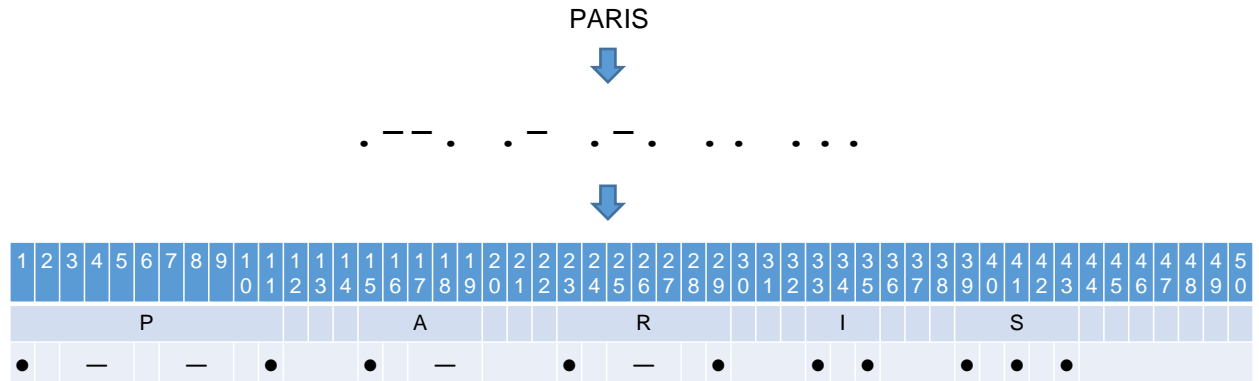
This highlights the relative gain of digital modes compared to conventional voice modes. The narrower digital bandwidth modes allow transmissions to have a higher signal to noise ratio (SNR) as less noise comes through with the transmission, allowing signals to be heard at greater distances in their communication links, while using less power in the process. The increase in efficiency for narrow bandwidth transmissions are substantial; for these reasons, QRP (reduced power) is a popular segment in the amateur radio hobby.

These benefits, however, come with their own trade trade-offs, mainly time. The relationship between bandwidth and time is inverse: the narrower the bandwidth, the longer it takes to send a message, or the more you slow a transmission, the less bandwidth you need. By way of analogy, a water balloon with a small pin prick hole in it will produce a very narrow focused stream, and it will take longer for the water to leave the balloon compared with water leaving the balloon through the wider nozzle at full force.

This can be illustrated using CW with a 100 Hz of typical bandwidth. Though not a true digital mode, the manually generated dits and dahs (i.e. dots and dashes) are “bit-like” and are ultimately reduced to

a series of “dits”. Timing in CW is relative to length of time it takes to make one dit, which represents one unit. A dah (or dash) proportionally represents 3 units. Spaces between dits and dahs making up one character are one space unit, and the space between each character of a word is 3 units. There are seven space units between words. International Morse code uses the word “PARIS” as the standard word for calibrating words per minute and conveniently has 50 units (dits). (<https://morsecode.world/international/timing.html>).

The conversion of “PARIS” to Morse Code to the 50 dits is detailed here:



Therefore, when one calculates the “dit speed” of someone sending a CW message at 12 words per minute (i.e. sending “PARIS” twelve times) the total number of dits sent in a 60 second period equals 600 (12 wpm x 50 dits/word). Dit speed is then calculated to be 60 seconds ÷ 600 dits, or 0.1 seconds/dits.

WSPR takes the efficiencies of narrow bandwidth to an even larger extreme. As a true digital model, WSPR actually generates four, 1.47 Hz signals within a 6 Hz bandwidth transmitting only 50 bits of information contained in a very minimal, one-way message including only the transmitter’s call sign, maidenhead grid locator, and power level in decibels. Specifically, WSPR messages are constructed as follows:

- 28 bits for call sign
- 15 bits for 4 digit maidenhead grid locator
- 7 bits for power level (db)

WSPR messages also contain extra bits for redundancy purposes and error correction in addition to using sophisticated algorithm encoding which allows WSPR transmissions to be very resistant to fading and interference. At the receiving station, the software is able to decode the message even if sections of the message are missing due to interference or suffer from some degree of frequency drift, and WSPR is able to decode transmissions with signal to noise ratios as low as -28 db (33).

For comparison purposes,

- The dit speed of CW at 12 wpm is calculated as:
 $= 12 * 50 = 600 \text{ dits} = 60 \text{ sec.} / 600 \text{ dits} = 0.1 \text{ second/dit}$
- The “effective bit speed” of a WSPR message is only 50 bits sent over 2 minutes and is calculated as:
 $= 120 \text{ sec.} / 50 \text{ bits} = 2.4 \text{ seconds/bit}$

Instead of transmitting 12 wpm as in the case of Morse Code, WSPR transmissions have a communication rate of effectively one word sent over two minutes. This means that when slowing the transmission time by sending a message with an effective bit rate of 2.4 seconds (as in the case of WSPR vs a comparative 0.1 second dits for CW), the bandwidth narrows and becomes a fraction of the Hertz of the frequency; improving the signal to noise ratio; this allows one to achieve worldwide communications with a fraction of a watt.

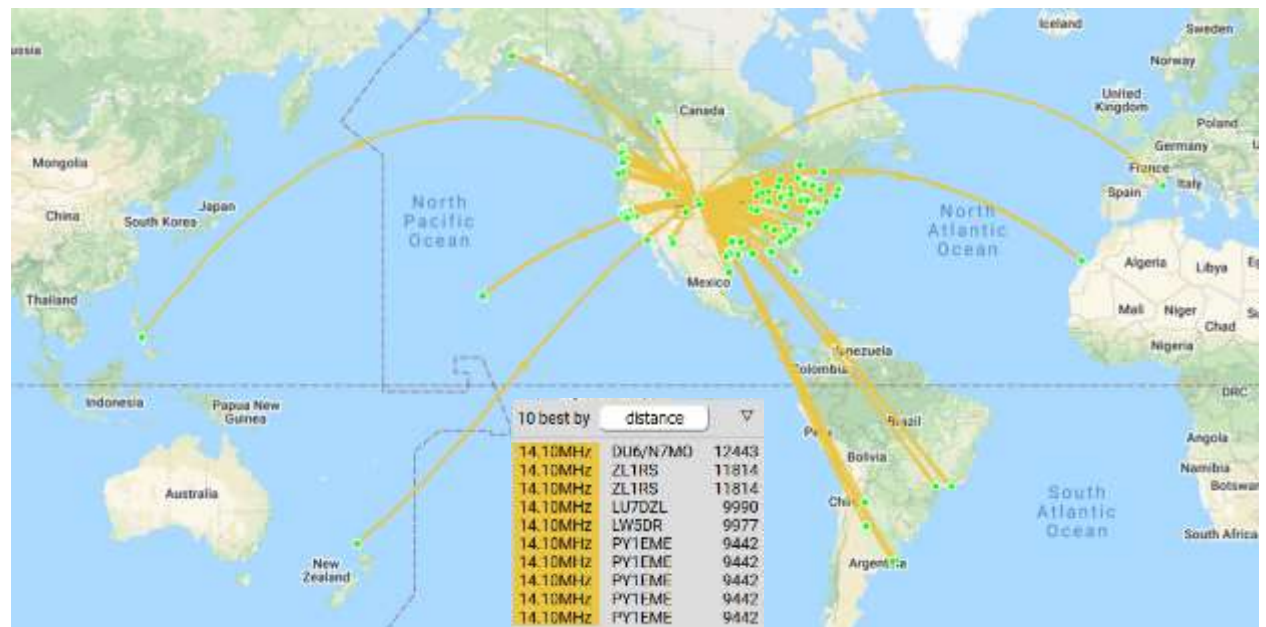
By understanding the efficiency gains of using narrow bandwidth, one can see the benefits of slowing transmissions to an extreme level. However, given the inverse relationship between bandwidth and time, there comes a point where it would be impracticable to decode signals manually and real-time digital signal processing software like WSJT-X, the software suite that contains the WSPR mode, would need to be used. The advantages of narrow bandwidth, low power transmissions really present themselves when using these sorts of transmissions as one-way beacon modes (as opposed to two-way communication modes); for this reason WSPR works well for the sorts of propagation experiments undertaken in this report.

C. Experiment – 20m Propagation Analysis

For one 24 hour period starting 3:15 PM MST, January 31, 2020 lasting until 3:15 PM MST, February 1, 2020, a series of WSPR transmissions were made under call sign W3LLA on the 20m band (14.0956 MHz) using a center-fed dipole antenna with 5 Watts of power. These transmissions were made from maidenhead grid DN70In (Ft. Collins, CO, USA) and were scheduled to occur at 20% intervals where, for every 10 minute period, one, two-minute transmission sequence was performed over a period of 24 hours. The 14 MHz frequency was chosen because it is a frequency which is above typical night-time MUF levels but below the daytime MUF levels. Accordingly, the resulting spots from a steady series of beacon transmissions sent at a fixed frequency at regular intervals over a 24 hour period would show a time response to Sun's movement; this would validate the diurnal effect of solar radiation on the ionosphere.

In this particular experiment, a total of 901 individual spots were made from 126 unique call signs with an average distance of 2,165 km over a 24 hour period.

Figure 25: WSPR transmissions (W3LLA, 1/31/20 to 2/1/20) - Spots



Source: <http://wspr.vk7jj.com/>

D. Results and Commentary

The purpose of this experiment was twofold: to visualize some of the dynamics of the ionosphere and to demonstrate the ionosphere's response to solar radiation and its impact on HF communication. If the electron count in the ionosphere responds immediately to fluctuations in solar radiation (e.g. the diurnal effects of the sun), then it can be reasonably assumed that real time WSPR spot reports of both

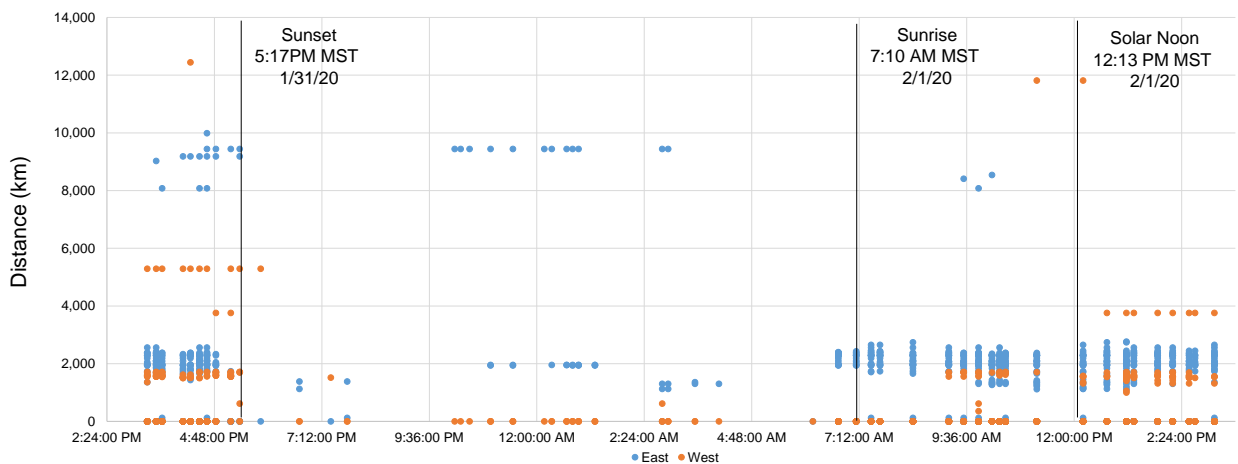
successful and unsuccessful communication links using the ionosphere would act as a sensor of some sort, and by extension illustrate something about the state of the ionosphere. With this in mind the results of this experiment are presented as a broad illustration of observations rather than as a highly quantitative analysis.

Recasting the spot results from the WSPRnet database to compare distance versus time, a picture emerges which shows the impact of the Sun on WSPR spot reports. In the chart below, the individual spots are plotted against time, with sunrise, sunset, and solar noon marked with vertical lines. All times in this chart are local to emphasise the daytime and night time periods. The individual spots themselves were color coded to indicate the directionality (east and west) relative to my position.

Firstly, keep in mind that the Sun tracks from east to west and the start of transmissions was at 3:14PM local time, close to sunset at 5:17PM. Accordingly, the Sun was to my west; therefore, one can see a large concentration of spots from the west. Additionally, the spot distances around sunset increased dramatically, likely because of “grey line” propagation; a dynamic where signals can travel great distances with little attenuation in locations simultaneously experiencing sunrise and sunset (34). After sunset, the number of spots drops off dramatically. As electron production slows/stops during the night, my transmission frequency of 14MHz exceeded the MUF, and the number of spots were noticeably limited.

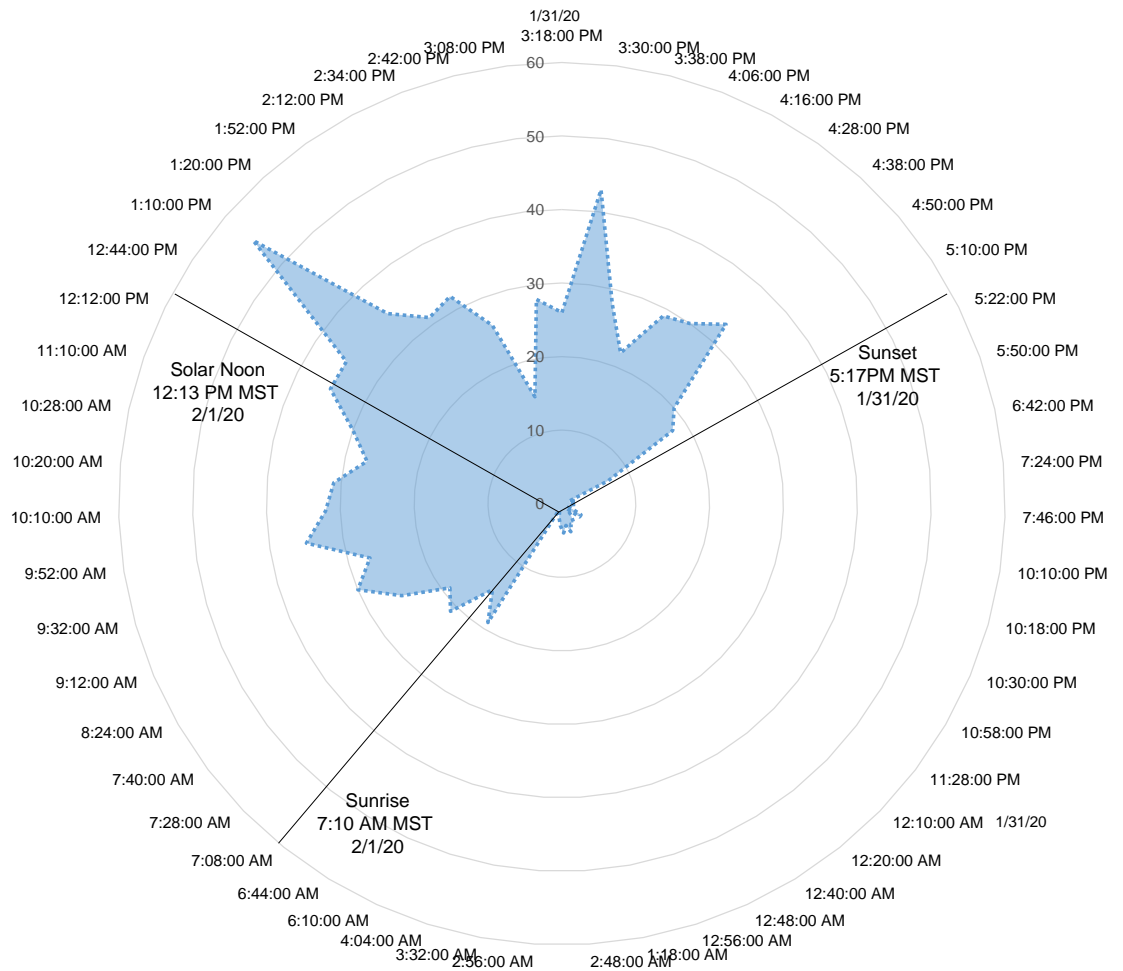
Approaching sunrise, with the Sun rising in the east, a marked increase in spots is noted right around the time of sunrise with a large concentration located to the east of my position. As the day progresses to solar noon, when the Sun is directly overhead, a mix of east and west spots begins to emerge. This shows the blend of spot count and direction tracking the east to west movement of the Sun, indirectly demonstrating the ionization of electrons in the ionosphere tracking the Sun exposure.

Figure 26: WSPR 24 Hour transmissions (W3LLA, 1/31/20 to 2/1/20) - Distance vs time (local time)



Source: W3LLA

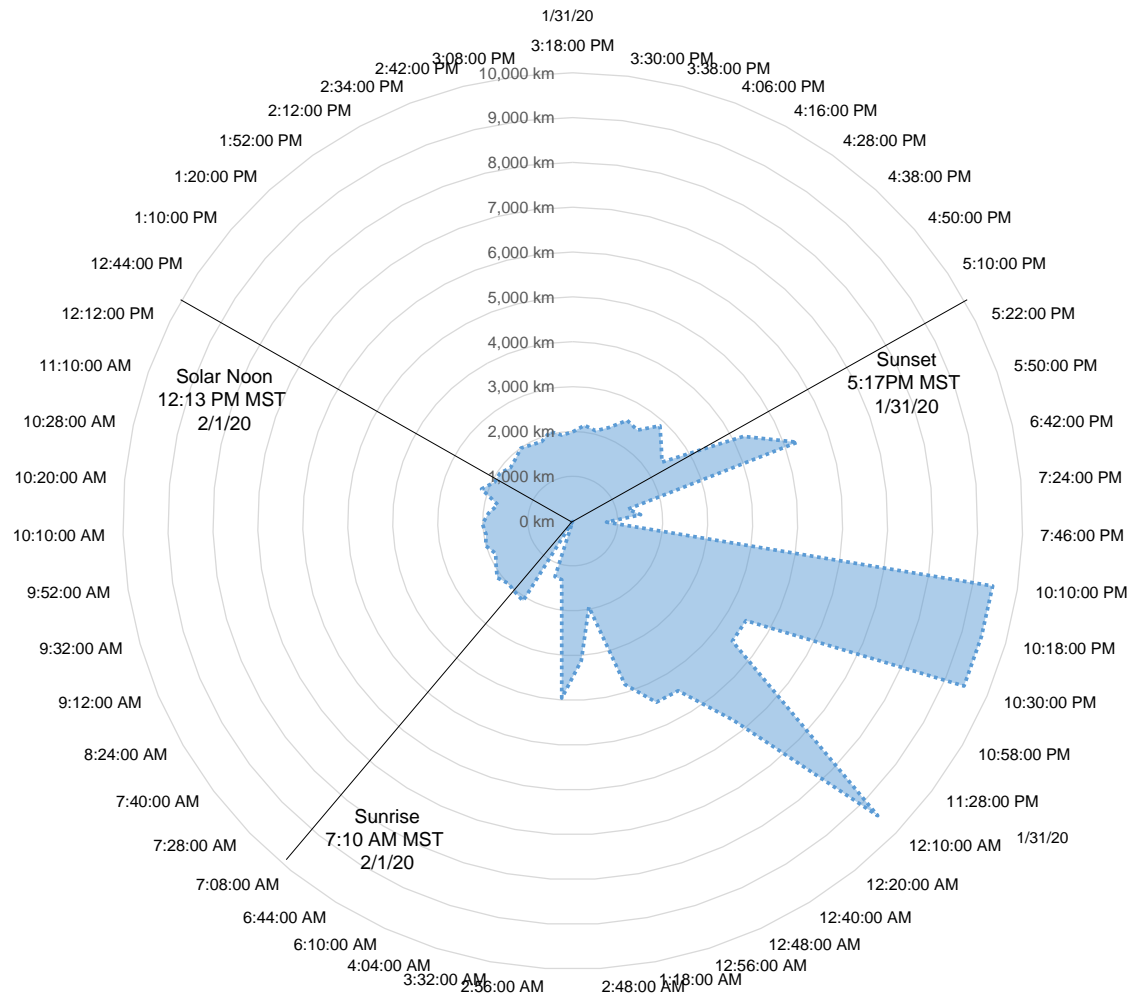
Figure 27: WSPR 24 Hour transmissions (W3LLA, 1/31/20 to 2/1/20) – Count per sequence vs time (local time)



Source: W3LLA

The chart above presents the number count of spots during each WSPR transmission sequence over the 24 hour period. The start and end point of the 24 hour cycle is located at the 12 o'clock position, and the transmission sequences are chronological and progress in a clockwise direction. In this presentation, the response of spot count to the diurnal impact of the Sun is evident. At night when the electron count in the ionosphere drops off, the 14MHz transmissions exceed the MuF, and substantially less contacts were made. What is interesting is how immediate the response is to sunset and sunrise. It is also evident that over the course of the day, spots gradually increase to a maximum count level until an hour after solar noon (when the Sun is most directly overhead) and then decreases as the Sun sets to the west.

Figure 28: WSPR 24 Hour transmissions (W3LLA, 1/31/20 to 2/1/20) - Average distance (km) per sequence vs time (local time)



Source: W3LLA

The chart above presents the average distance of the spots during each two minute WSPR transmission sequence over the 24 hour period. In this presentation, one can see the consistent average distances during the daytime period hovering around 2,000 km and a steady increase and spike in distances towards sunset. Viewing this together with the maximum skip distances presented in section II.H Expanded Model, Table 3, it is easy to visualize the impact of the lower D and E Layers on the skip distances during the day and how, when the Sun sets, transmissions can access the upper ionospheric layers and thus achieve further skip distances. During the night, the large distances achieved are from one single station 9,442 km away in Rio de Janeiro. This spot is somewhat anomalous and might have benefited from grey line propagation effects.

E. WSPR Propagation in Relation to Ionosonde Critical Frequency Readings

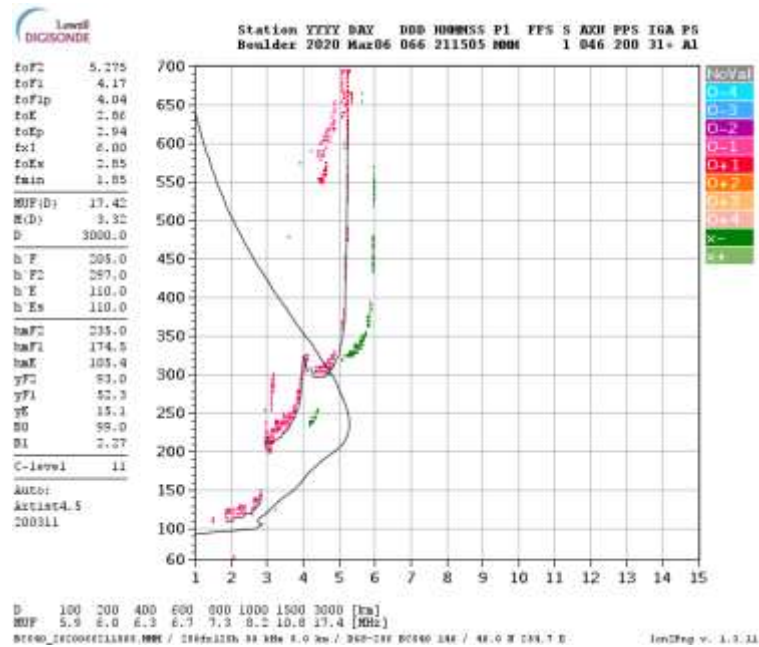
For a 24 hour period starting at 1:20 PM MST, March 6, 2020, lasting until 1:20 PM MST, March 7, 2020, a series of WSPR transmissions were made under call sign W3LLA on the 20m band (14.0956 MHz) using a center-fed dipole antenna with 5 Watts of power in the same configuration as the experiment in Section III.C Experiment – 20m Propagation Analysis . These transmissions were made from maidenhead grid DN70In (Ft. Collins, CO, USA) and were scheduled to take place for two minutes for every ten minute period. A total of 2,252 individual spots were made and analysed.

In this particular experiment, the WSPR propagation reports are presented against periodic measurements taken by the vertical incidence ionosonde at Boulder, CO: the critical frequency (FoF2) and the height of the F and E layers. As mentioned before, the 14 MHz frequency was chosen because it is a frequency which is above typical night-time MUF levels but below the daytime MUF levels. Accordingly, the resulting spots would show a strong time response to Sun's movement. By extension then, the spots would also show a time response to the changes in critical frequency and the altitude of ionospheric layer where incidence occurs as these are directly impacted by solar radiation.

It should be noted that the critical frequency of the Boulder Ionosonde is a measure of vertical incidence directly above the station, approximately 50 miles from W3LLA station. Comparing the measurements of Boulder Ionosonde to WSPR spots which are hundreds and thousands of miles from W3LLA station is a somewhat apples to oranges comparison given that the point of ionospheric incidence for the WSPR transmissions are some distance from both W3LLA and Boulder stations. The Boulder station provides information about the ionosphere directly above Boulder while WSPR transmissions are oblique measures of the ionosphere at some midway point between the transmitter and receiver location. Despite these differences, the time response relationship between distant WSPR spots and the Critical Frequency of Boulder Station is still evident.

For this analysis, 24 separate ionograms from the Boulder Ionosonde were compiled for the beginning of each hour of the WSPR transmission experiment. The critical frequency (FoF2) and ionospheric layer heights, h'F and h'E, we compared against the WSPR spots over time (see illustrative ionosonde report from the Boulder ionosonde Figure 29).

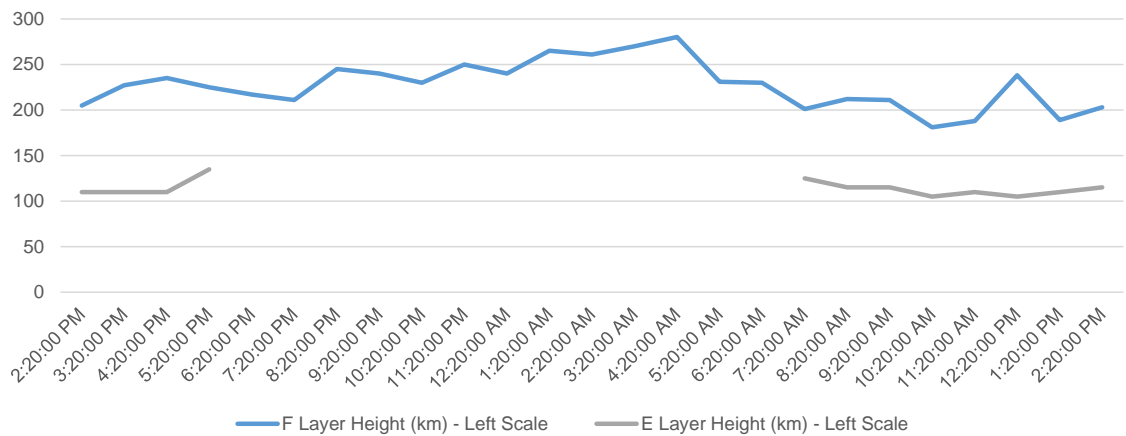
Figure 29: Illustrative Ionogram from Boulder station



Source: <ftp://ftp.ngdc.noaa.gov/ionosonde/data/BC840/individual/2020/066/image/>

From the ionograms, the following ionospheric layer heights in kilometres were compiled representing hourly measures over a period of 24 hours.

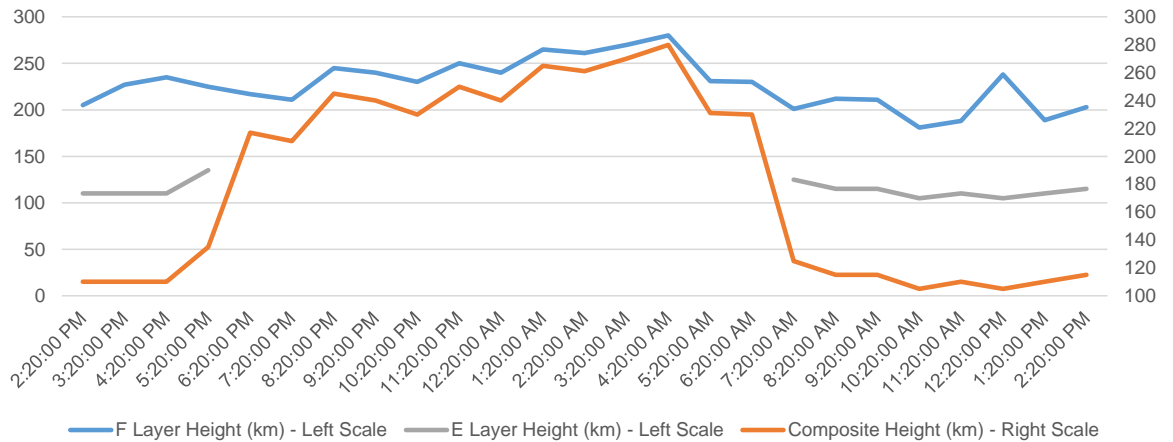
Figure 30: Boulder Station Ionospheric Layer Heights (local time)



Source: W3LLA & NOAA data

For illustrative purposes, a third line was added (Figure 31) which is a composite of the F and E-layer heights. The idea behind this was to illustrate a single ionospheric “ceiling” and its altitude over the course of the experiment. For the periods where the E-layer was present, the E-layer height was used. For the post sunset and pre-sunrise periods, where no E-layer heights were provided from the Boulder Ionosonde, the F layer height was used.

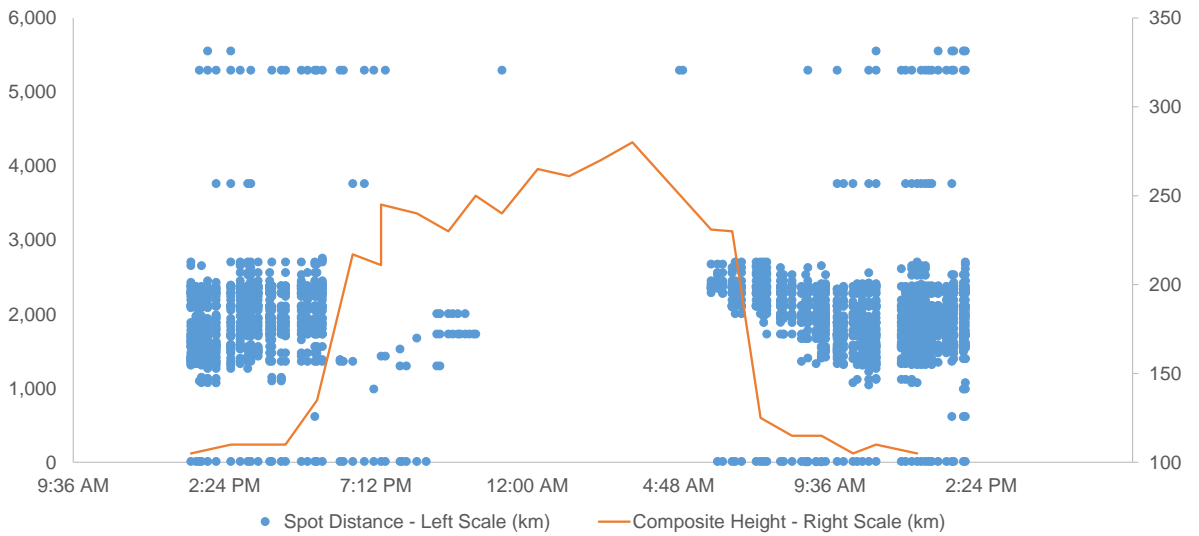
Figure 31: Boulder Station Ionospheric Layer Heights with Composite Height (local time)



Source: W3LLA

When comparing the WSPR spot distances against the composite ionospheric height it is possible to see the attenuating impact that the lower ionosphere layers have on WSPR spot distances. The chart below (Figure 32) shows both the gradual increase in spot distances after sunset and the reduction in spot distances after sunrise, as the lower E layer is activated.

Figure 32: WSPR 24 Hour Spots (3/6/20 to 3/7/20) Against Composite Ionospheric Height (km)

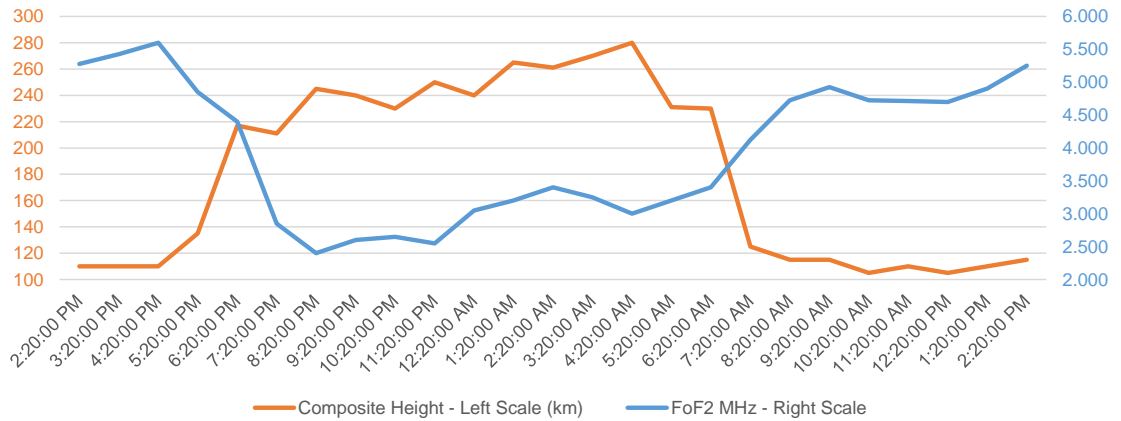


Source: W3LLA

Note: Excludes spots with distances greater than 6,000 km

It is also interesting to note the period around midnight where no spots were recorded as the transmission frequency of the WSPR signals at 14MHz exceeded the MuF. The chart below shows the Critical Frequency at the Boulder Ionosonde over the same period.

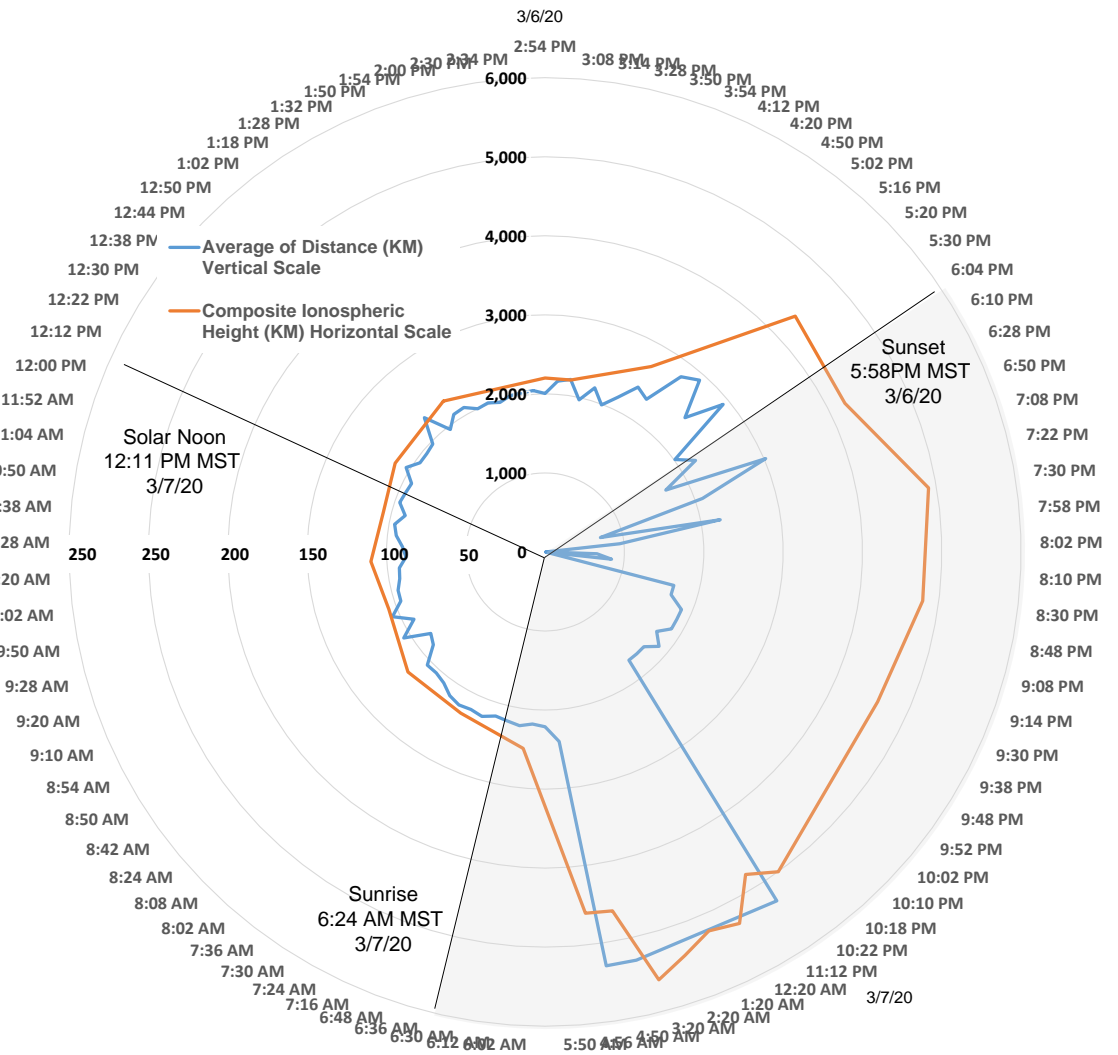
Figure 33: WSPR 24 Hour transmissions (W3LLA, 3/6/20 to 3/7/20) - Distance vs time (local time)



Source: W3LLA & NOAA

The chart below presents the same data but in a 24 hour clockwise time sequence. The start and end point of the 24 hour cycle is located at the 12 o'clock position, the transmission sequences are chronological and progress in a clockwise direction. The average spot distance during the WSPR transmission sequences shows a clear relation to the composite ionospheric height (e.g. the indicative altitude where incidence most likely occurred during skip transmissions). During the daytime hours, the average distances are lower in the presence of a lower ionospheric layer, while average distances are higher near sunset and during the night where the higher F layer is active.

Figure 34: WSPR 24 Hour transmissions (W3LLA, 3/6/20 to 3/7/20) – Average Spot Distance per Transmission Sequence and Composite Ionospheric Height vs time (local time)



Source: W3LLA

F. Heat Mapping WSPR Data

WSPR stations can be thought of as a series of sparsely distributed oblique sensors of the ionosphere, collecting information of successful communication links using ionospheric skip at various frequencies. If skip communication is successful on any particular frequency for a desired distance, it is because ionospheric conditions permitted it; therefore, the band is deemed to be “open”.

Given that the electron count in the ionosphere responds immediately to solar phenomena like solar flares, the 11-year sunspot cycle, and the diurnal effects of the Sun, it stands to reason that communication links using the ionosphere infer something about the state of the ionosphere, and that real time spot reports of successful communication links like those contained in the WSPR Database, act as an indirect sensor of these phenomena.

Below is a spot report for W3LLA station on 14MHz for 24 hours. It shows the spots of one transmitter (Tx) and all receiving stations (Rx) for one 24 hour period starting 3:00 PM MST, February 28, 2020 lasting until 3:00 PM MST, February 29, 2020, using the same center-fed dipole antenna configuration and power settings as in Section III.C above.

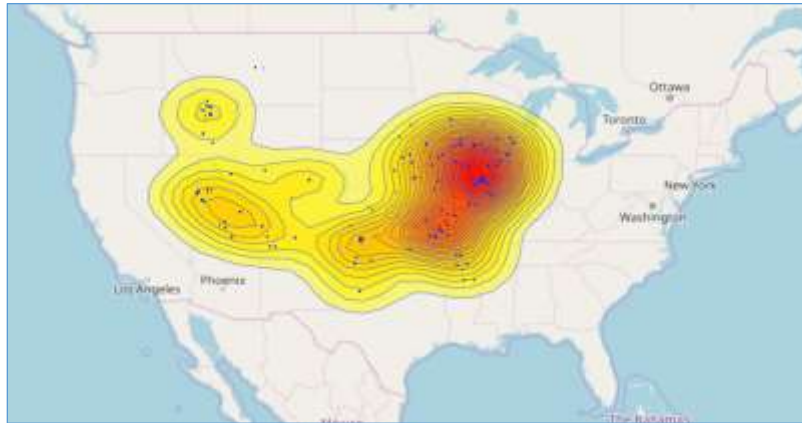
Figure 35: WSPR transmissions (W3LLA, 2/28/20 to 2/29/20) - 24 Hour Spots



Generated from: <http://wspr.vk7jj.com/>

Using this series of WSPR spots taken over a 24 hour period, a heat map was created that visually depicts the geographic zones where the signals could theoretically have entered the ionosphere after making an assumption for the number of skips in the communication link.

Figure 36: WSPR transmissions (W3LLA, 2/28/20 to 2/29/20) - 24 Hour Heat Map



Generated from: <http://www.heatmapper.ca/geocoordinate/>

In this particular heat map, it was assumed that each reception report entailed only one skip; therefore, the heat zones on the map represent the geographic mid-point between the transmitter location and the location of the receiving station over a 24 hour period. What this analysis lacks in precision, it makes up for in visual impact. In this experiment, approximately 1,900 separate spots were made over a 24 hour period. Time-lapsing the midpoint locations and clustering them based on proximity illustrates the migration of zones of increased electron count in the ionosphere in relation to diurnal changes, tracking east to west (see Figure 35). This implies that for any particular midpoint location, the Maximum Usable Frequency was, at the very least, higher than 14 MHz, the transmitted frequency for this particular experiment. Making an assumption for likely ionospheric layer altitude, angles of incidences of the signal could be determined and potentially “range bound” an assumption for electron count at altitude.

This heat map is a modeled representation of the virtual reflection points of the signal in the ionosphere, and it can be considered to be an indirect and oblique sounding of the ionosphere itself. Though approximate and imprecise, the sheer number of points from one transmitter over a time-lapsed 24 hour period is instructive and demonstrates the ebbing and flowing of the electron count in the ionosphere at various altitudes in response to the diurnal changes in solar radiation.

For demonstration purposes, comparing the heat map in Figure 36 to the path of the Sun over the Earth's surface during the day of the experiment "loosely" tracks the 24 Hour Heat Map.

Figure 37: Sun Tracking Path (Ft. Collins, CO 2/28/20 to 2/29/20)



Source suncalc.org

As detailed earlier, the WSPR Database reports the location of each station using the Maidenhead Grid Locator. To determine the midpoint latitude and longitude between the W3LLA transmitting station (located at Maidenhead Grid DN70In) and the receiving spotting locations, the Maidenhead Grids from WSPR were converted into latitude and longitude. For this, I used the Excel based Visual Basic macros made by KK6MK (located at <http://www.xertech.net/Projects/DistBear.html>)

Once the latitude and longitude of each spot were obtained, the distance between the transmitting and receiving stations and the latitudes and longitudes of the midpoint locations between them was calculated. To determine the distance, the Haversine formula was used to find the great-circle distance (i.e. the shortest distance between the two points on a sphere). To determine the distance incorporating the latitude and longitude coordinates the following was used (35):

$$a = \sin^2(\Delta\phi/2) + \cos \phi_{T_x} \times \cos \phi_{R_x} \times \sin^2(\Delta\lambda/2) \quad [90]$$

$$c = 2 \times \text{atan2}(\sqrt{(1-a)}, \sqrt{a}) \quad [91]$$

$$d = R \times c \quad [92]$$

Where ϕ is latitude, λ is longitude, T_x is the transmitting station, R_x is the receiving station, R is the Earth's radius (volumetric mean radius = 6,371km) and $c = 2 \times \text{atan2}(x,y)$.

For example, the distance between W3LLA station located at DN70ln (Ft. Collins, CO) and FN10nw (the Olin Science Building at Bucknell University in Lewisburg, PA) would be calculated as follows:

Station	Maidenhead Grid	Location	Degrees		Radians	
			Lat ϕ	Lon λ	Lat ϕ	Lon λ
T _x	DN70ln	Ft Collins, CO	40.5625	-105.0417	0.7079	-1.8333
R _x	FN10nw	Bucknell Univ.	40.9375	-76.8750	0.7145	-1.3417

Using the equation:

$$a = \sin^2(\Delta\phi/2) + \cos \phi_{T_x} \times \cos \phi_{R_x} \times \sin^2(\Delta\lambda/2) \quad [93]$$

Where $\Delta\phi$ and $\Delta\lambda$ are:

$$\Delta\phi = 40.9375^\circ - 40.5625^\circ = 0.3750 = 0.0065 \text{ Radians} \quad [94]$$

$$\Delta\lambda = -76.8750^\circ - (-105.0417^\circ) = 28.1667 = 0.4915 \text{ Radians} \quad [95]$$

With angles converted to radians:

$$a = \sin^2\left(\frac{0.0065}{2}\right) + \cos 0.7079 \times \cos 0.7145 \times \sin^2\left(\frac{0.4915}{2}\right) = 0.0340 \quad [96]$$

$$c = 2 \times \text{atan2}(\sqrt{(1 - 0.0340)}, \sqrt{0.0340}) = 0.3709 \quad [97]$$

Where the two-argument inverse tangent function is expressed as $\text{atan2}(x, y)$.

Then the great-circle distance is calculated as:

$$d = R \times c \quad [98]$$

$$d = 6,371\text{km} \times 0.3709 = 2,363\text{km} \quad [99]$$

To generate the heat map, it was assumed that the area where the signal entered the ionosphere (i.e. the apparent reflection point) was the midpoint location between the transmitting station and the receiving station. This was assumed for the spots that fell within typical single skip distance of less than 4,000km. While the precise location (or path) of where or how any particular signal entered the ionosphere cannot be precisely determined, the purpose of this exercise was to graphically illustrate the migration of successful WSPR spots in relation to the transmitter's geographic location over a period of 24 hours.

To calculate the midpoint latitude and longitude between the receiving and transmitting station the following formulas were used.

$$B_x = \cos \varphi R_x \times \cos \Delta\lambda \quad [100]$$

$$B_y = \cos \varphi R_x \times \sin \Delta\lambda \quad [101]$$

$$\varphi \text{ midpoint} = \text{atan2} \left(\sqrt{(\cos \varphi T_x + B_x)^2 + B_y^2}, \sin \varphi T_x + \sin \varphi R_x \right) \quad [102]$$

$$\lambda \text{ midpoint} = \lambda T_x + \text{atan2}(\cos(\varphi T_x) + B_x, B_y) \quad [103]$$

Where φ is latitude, λ is longitude for the respective the receiving station (R_x) or transmitting station (T_x) and where $\Delta\lambda$ is:

$$\Delta\lambda = -76.8750^\circ - (-105.0417^\circ) = 28.1667 = 0.4915 \text{ Radians} \quad [104]$$

Therefore:

$$B_x = \cos 0.7145 \times \cos 0.4915 = 0.6660 \quad [105]$$

$$B_y = \cos 0.7145 \times \sin 0.4915 = 0.3566 \quad [106]$$

Using Excel to calculate the midpoint latitude in decimal degrees we have:

$$\begin{aligned} \varphi \text{ midpoint} &= \text{atan2} \left(\sqrt{(\cos 0.7079 + 0.666)^2 + 0.3566^2}, \sin 0.7079 + \sin 0.7145 \right) \quad [107] \\ &= 0.7263 \text{ Rad} \times \left(\frac{180}{\pi} \right) = 41.6145^\circ \end{aligned}$$

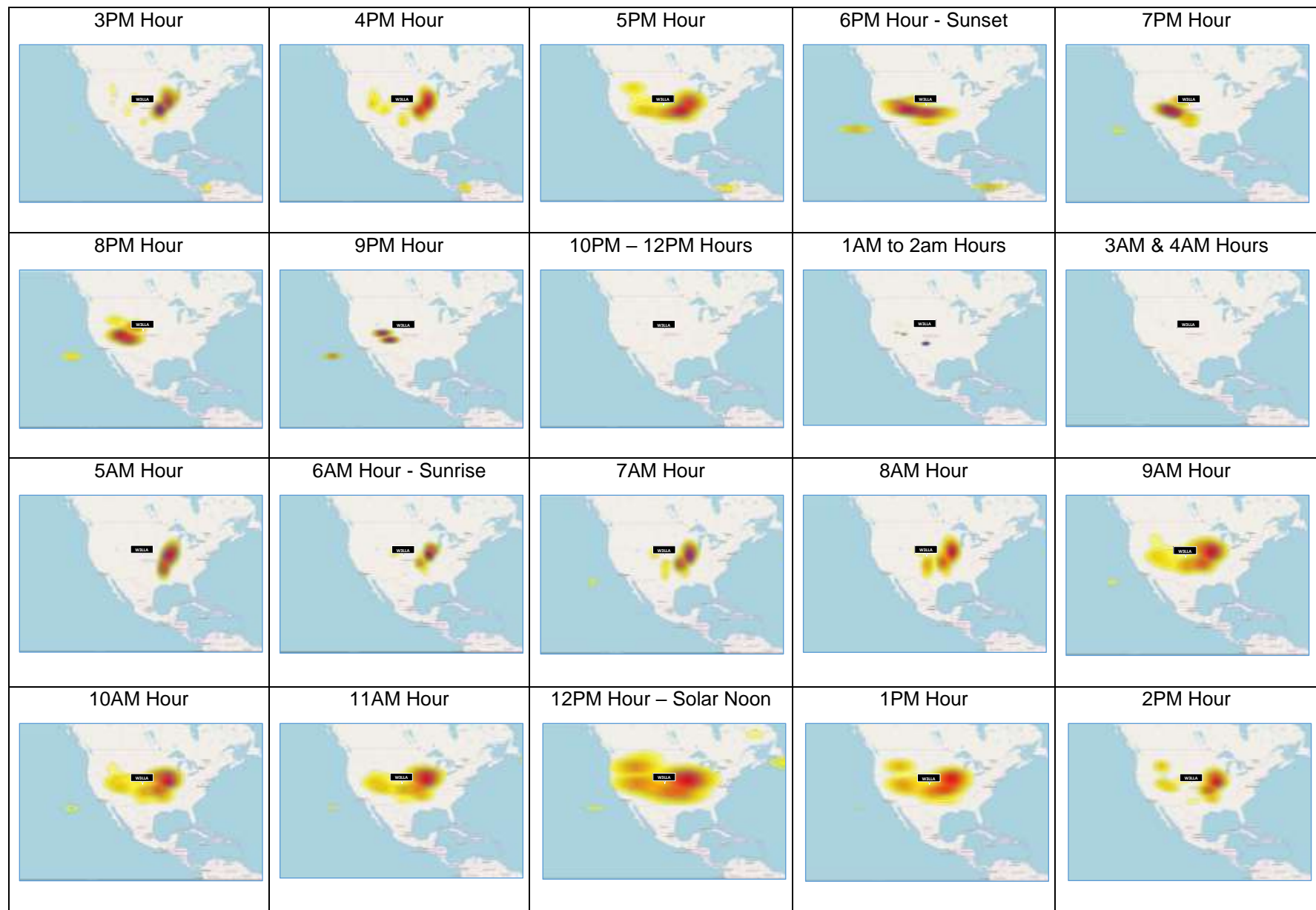
To calculate the midpoint longitude we have:

$$\begin{aligned} \lambda \text{ midpoint} &= -1.8333 + \text{atan2}(0.3566, \cos(0.7079) + 0.6660) \quad [108] \\ &= -1.5882 \text{ Rad} \times \left(\frac{180}{\pi} \right) = -91.9972^\circ \end{aligned}$$

Once the midpoint latitudes and longitudes for the spots were calculated, an excel file containing the grid coordinates was uploaded to the website <http://www.heatmapper.ca/geocoordinate/> which mapped the points and clustered the points based on a number of assumptions, which includes a Gaussian Radius Multiplier which refers to the width of groupings of points (36).

In Figure 35, a series of heat maps are assembled in an hourly time-lapse presentation. The start of the 24 hour transmission experiment begins at 3PM local time and proceeds in sequential time increments from left to right. What is noticeable from this presentation is the clear movement of the heat cloud from east to west broadly tracking the movement of the sun with the highest concentration “heat” occurring during the hour of solar noon.

Figure 38: WSPR 24 Hour transmissions (W3LLA, 2/28/20 to 2/29/20) – Mid Point Spot Heat Cluster (local time)



IV. Signal Propagation Mathematics – Colorado State University Project

A. Overview

This project is a summary of a project I submitted to the Colorado State University Math Day Competition in November, 2019. Also included in this project was a discussion of skip distance using the simplistic model outlined in Section 0.

This experiment compares the propagation pattern of a horizontal dipole antenna at different heights.

1. I construct a dipole antenna and use a free software package, MMANA-GAL, to model its radiation pattern.
2. I will transmit a series of short beacon signals using a transceiver. Other radio operators from around the world that pick up these signals will automatically report the contact to the Weak Signal Propagation Reporter (WSPR), an open source reverse-beacon network.
3. I will analyze and compare the signal reports generated for each antenna height against each other to determine which sends signals further.

My independent variable is the antenna height, and my dependent variable is the distance of the reporting station.

B. Hypothesis

Spots from the higher antenna would go further because the higher the antenna, the lower the take-off angle that the maximal strength signal radiates from the antenna, and therefore the signal will travel further as it enters the ionosphere at a greater angle of incidence and at a greater distance from the signal's origin.

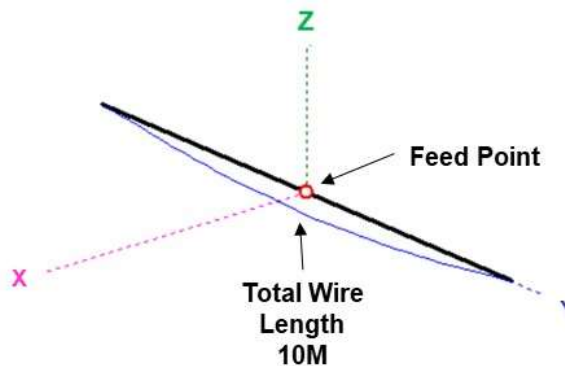
C. Construct

I constructed a 20m, center-fed dipole antenna. The antenna was made of two equal lengths of 14 gauge copper wire which were approximately $\frac{1}{4} \lambda$ in length each. These elements are connected in the center by coaxial cable, which connects to my transceiver. My antenna is tied between two trees, and I am able to move it up and down.

D. Model

I modeled a 20m dipole antenna in MMANA-GAL antenna modelling software. This free software allowed me to generate propagation patterns of the antenna's signal from an overhead, elevation and 3D viewpoint. From this model, I was able to estimate the angle of maximum directional gain of an antenna's signal at different heights, which helped me estimate which configuration will go further.

Figure 39: 3D view – dipole antenna



Source: Antenna schematic created by Maxwell Moran, W3LLA using MMANA-GAL Software

E. Transmit

I ran a series of ≈ 2 minute long WSPR transmission sequences on a HF transceiver on the 20m band (14MHz) using a dipole antenna at two different heights, one at $1/3$ wavelength (λ) above the ground and the other at $1/8 \lambda$. These one-way, beacon-like signals are very narrow in bandwidth and only include my call sign, location, and power in decibels (dB) (e.g. W3LLA DN70 37). After each cycle, signal reports from other radio operators (spotters), are automatically posted to the WSPR database for analysis.

The QRP Labs QCX is an example of a cheap (\$49) transceiver which I constructed and hand soldered. In its intended design, the QCX is only a WSPR transmitter, however, I designed and published a modification to allow the QCX to receive signals making it a pure transceiver. QRP Labs published this modification on their website, which is located here: <http://www.qrp-labs.com/qcx/qcxmods/qcxwspr>

Figure 40: QRP Labs, QCX Transceiver



Source: W3LLA

F. Analyze

I analyzed the data from the WSPR database using a spreadsheet (e.g. LibreCalc or Excel) to see if there was a noticeable difference in spot distance if I changed the height of my antenna.

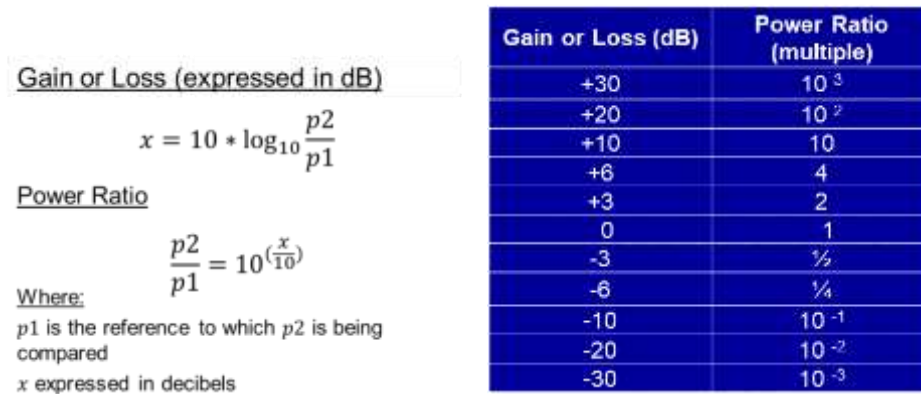
The WSPR database lists the distance and the directional azimuth from my position to all of the radio operators who heard my beacon (spots). To make this analysis visually meaningful, I plotted the spots on a Cartesian plane rather than relying on WSPR's mapping function. To do this, I converted the WSPR spot data (provided in polar coordinates) to rectangular coordinates by using trigonometry, and I plotted the points in Excel using a scatter chart.

G. Antenna Modeling

One purpose of antenna modeling is to illustrate the radiation pattern of a specific configuration. Signal strength/weakness in any direction is expressed as a gain/loss compared to an antenna floating in free space, or an isotropic antenna. This gain is expressed in decibels (dBi), a base ten logarithm.

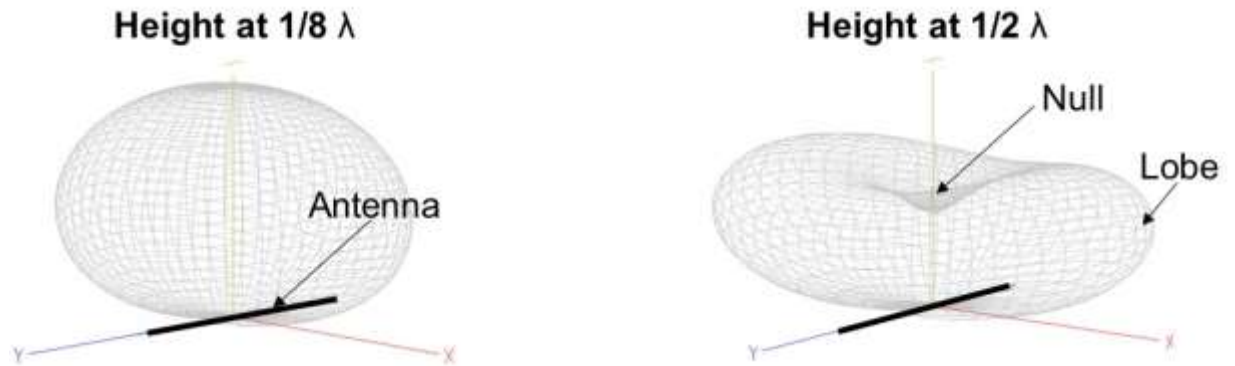
For example, a gain of 3 dBi has 2 times more gain than an isotropic antenna while a gain of 10 dBi has a gain of 10 times.

Figure 41: Decibel relation to power ratio



In a dipole antenna the signal propagates broadside to the wire element and the radiation patterns create lobes and nulls of varying signal intensity as the antenna is raised or lowered.

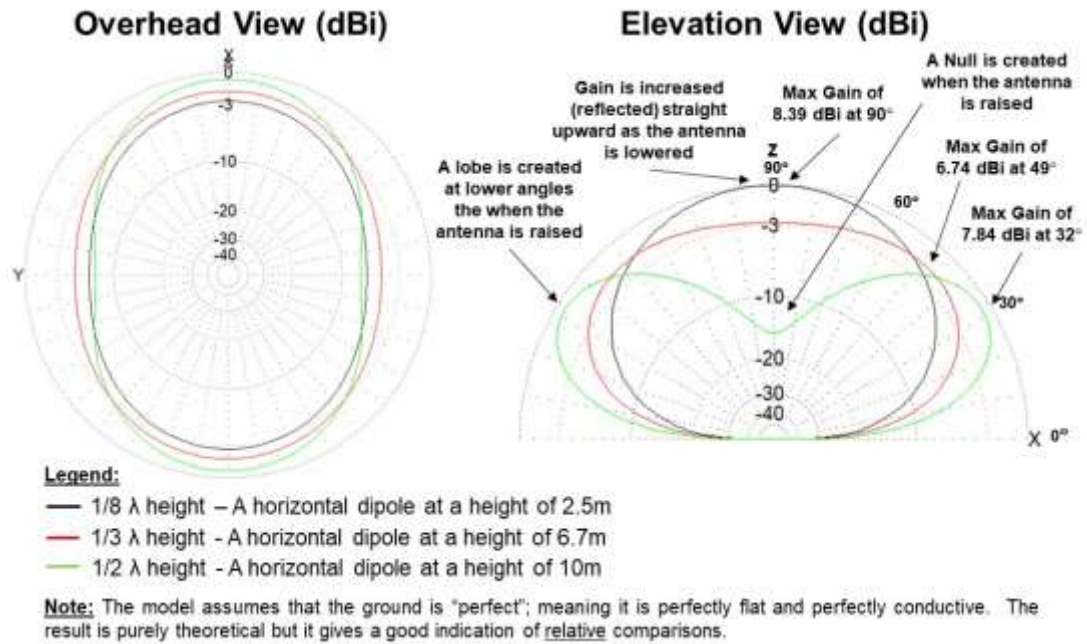
Figure 42: 3D view of the propagation pattern of a dipole at different heights



Source:W3LLA & MMANA-GAL

I modelled three configurations using the MMANA-GAL software. The figures below are the far field charts which compare the field strength, expressed in dBi, of a signal at some distant point relative to an isotropic antenna (a purely theoretical and omnidirectional antenna in free space).

Figure 43: Antenna radiation patterns at different heights



Source: W3LLA & MMANA-GAL

The $1/3 \lambda$ antenna is 4.7x stronger than an isotropic antenna at an elevation of 49° and the $1/8 \lambda$ antenna is 6.9x stronger at 90° (directly above).

One will notice from the far field figures above the creation of lobes and nulls in the radiated pattern as an antenna is raised or lowered. "These formations arise from the reflection of the antenna's radiated energy by the ground....the actual radiation pattern is composed of energy received directly from the antenna and energy that has been reflected from the ground. The direct and reflected signals take different amounts of time to get to the receiving station so they can add together, cancel each other out, or any combination in between."

(12)

"The higher the horizontal antenna, the lower is the

lowest lobe of the pattern. As a very general rule of thumb, the higher an HF antenna can be placed above the ground, the farther it will provide effective communications because of the resulting lower radiation angle. This is true for any horizontal antenna over real and well as theoretically perfect ground."

(7)

Height	$1/8 \lambda$	$1/3 \lambda$	$1/2 \lambda$
Max Gain	8.39 dBi	6.74 dBi	7.84 dBi
Elevation Angle of Max Gain	90°	49°	32°
Gain(x) $\frac{p2}{p1} = 10^{(\frac{x}{10})}$	6.9x	4.7x	6.1x

H. WSPR Background

WSPR (pronounced "whisper") stands for "Weak Signal Propagation Reporter" and was created by Dr. Joe Taylor, K1JT, Nobel Laureate (Physics, 1993). This program is designed for sending and receiving low-power transmissions to test propagation paths mainly on the High Frequency (3-30 MHz) bands.

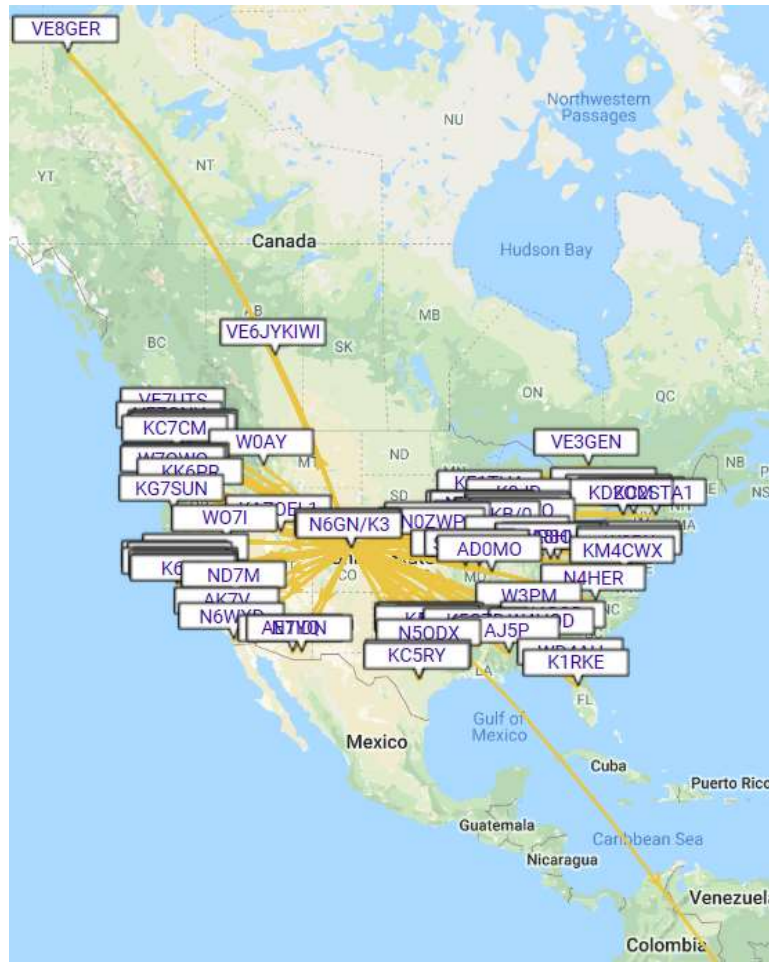
- Designed for one way, minimal contact (call sign, location, & power level).
- Each WSPR transmission cycle lasts one minute and 50 seconds and at the end of each cycle, the signal reports are posted to the internet database.
- WSPR transmissions are a low power, very narrow bandwidth mode (6 Hz). I generated these transmissions using only 5 Watts.

On June 15, 2019, I conducted a series of WSPR transmissions using a 20m dipole at two heights, $1/3 \lambda$ and $1/8 \lambda$. I chose these heights because the highest I could make my antenna was only 22 feet ($1/3 \lambda$). I ran my transmissions on the 20m (14 MHz) band.

I ran my transmissions for approximately 45 minutes before noon and 45 minutes after noon with a brief pause in the middle to change the height. In total, I ran a series of 21, two minute cycles at each height, totalling 42 minutes of total transmission time over 90 minutes.

The WSPR database lists the distance and the directional azimuth from my position to all the radio operators who heard my beacon (spots). I downloaded the WSPR data into Excel, and I plotted the spots on a Cartesian plane (scatter chart) by converting the WSPR spot data (provided in polar coordinates) to rectangular coordinates by using trigonometry. I also inverted the x and y axis to fix the 0° mark to be on the top (i.e. the north position).

Figure 44: Total WSPR spots 20m band



Source: <http://wspr.vk7jj.com/>

Table 5: Example spreadsheet calculation

WSPR Data		Direction, Θ	Plot Coordinates		Inverted	
Distance, r	Azimuth	Azimuth $^\circ \times \pi/180$	$r \cdot \cos(\Theta)$	$r \cdot \sin(\Theta)$	x	y
1,501	261	4.56	(235)	(1,483)	(1,483)	(235)
1,171	82	1.43	163	1,160	1,160	163
1,554	296	5.17	681	(1,397)	(1,397)	681
1,469	80	1.40	255	1,447	1,447	255
2,374	74	1.29	654	2,282	2,282	654

In total, I had 528 spots from 115 spotters during 21, two minute transmission sequences over a period of an hour and a half.

I. WSPR Field Test Results

Figure 45: Total WSPR Spots at $1/8 \lambda$ (Low Height) – KM & Azimuth

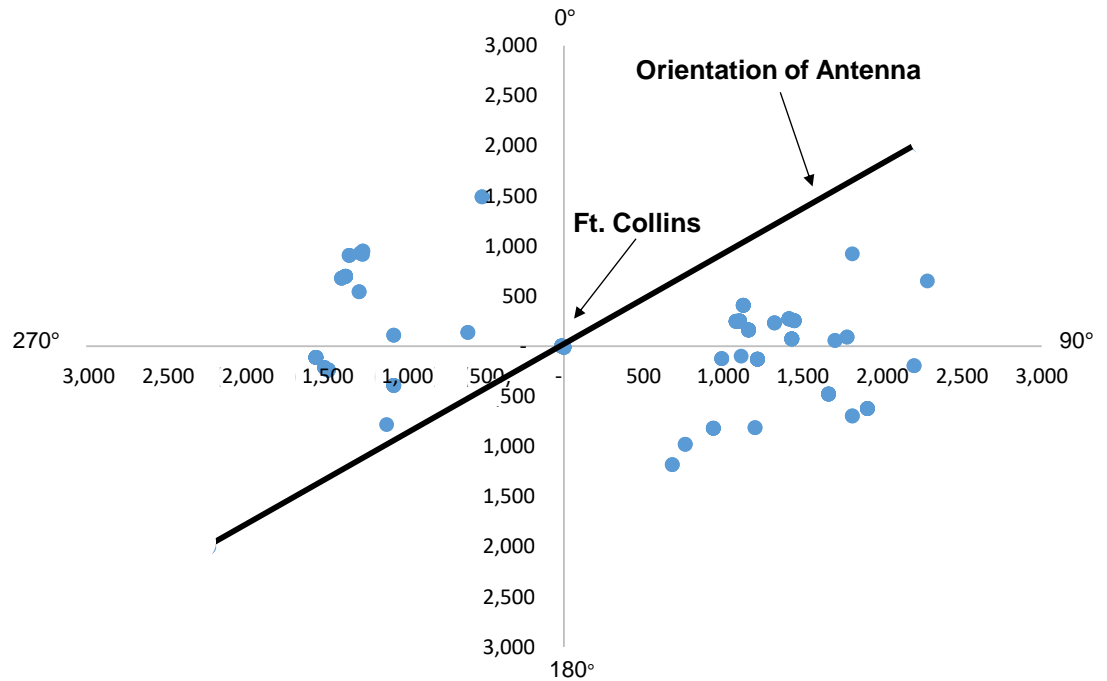


Figure 46: Total WSPR Spots at $1/3 \lambda$ (High Height) – KM & Azimuth

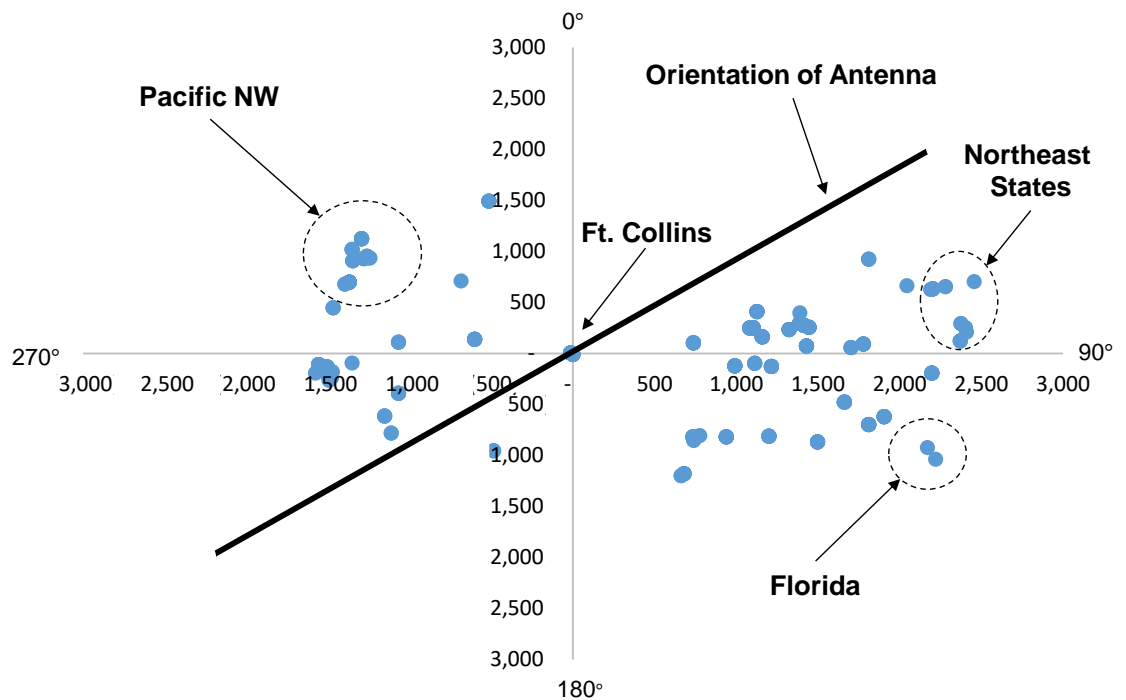


Table 6: Field test results

Distance	1/8 λ		1/3 λ	
	Spot Count	%	Spot Count	%
0 - 499 km	22	12%	20	6%
500 - 999 km	5	3%	26	8%
1,000 - 1,499 km	93	51%	150	43%
1,500 - 1,999 km	52	29%	108	31%
>= 2,000 km	10	5%	42	12%
Total Spots	182		346	
Average Distance km	1,250		1,419	
WSPR Transmission Sequences	10		11	
Number of spotters	43		72	
Average Spots per Spotter	4		5	
Average spots per transmission sequence	18		31	

Note: The near field (<500km) spots were mostly closer than 15km away and were likely a result of ground skip propagation, not sky wave.

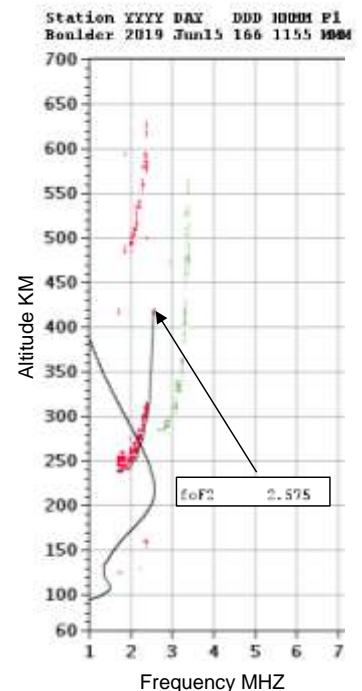
J. Summary Conclusions

The results of my experiment are consistent with my hypothesis. When the dipole was raised:

- The average distance of the spots increased from 1,250km to 1,419km, an increase of 14%.
- The total number of spots increased from 182 to 346, a 90% increase, and the total number of spotters from 43 to 72, a 67% increase.
- The average number of spots per transmission cycle increased by 73% from 18 spots to 31 spots per transmission.

Interestingly, I noticed that raising the antenna resulted in an almost doubling in the overall spot count, while lowering the antenna did not necessarily show more near field spots:

- This may be due partly to the fact that the population density of the East and West Coast is much greater than in a 1,000km radius around Ft. Collins, CO.
- More likely, it is because my signal frequency of 14MHz exceeded the Maximum Usable Frequency (MUF) overhead, and my signals probably passed through the ionosphere for the area directly above my position, limiting spots closer to me. One can see from the vertical incidence ionogram produced from the Boulder, CO ionosonde (approximately 50 miles from my location) that the critical frequency at the time of my test maxed out at 2.575MHz.

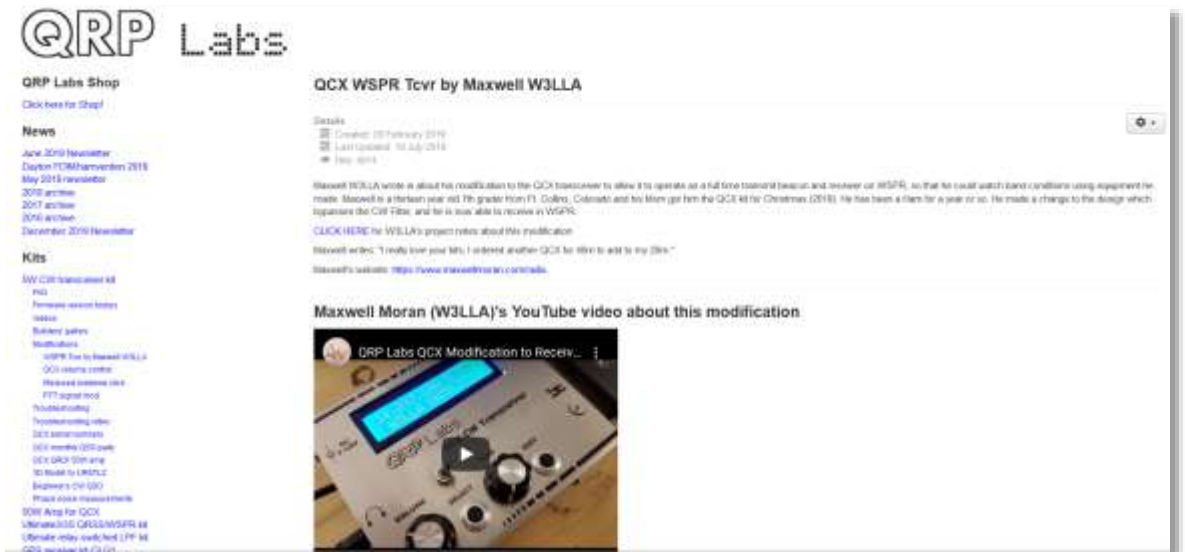


V. Modification of the QRP Labs QCX CW Transceiver

A. Introduction

This project titled “Modification of the QRP Labs QCX CW Transceiver - CW Filter Bypass to Receive Transmissions in WSPR Mode” was published on January 30, 2019. This modification was published in QRP Labs’ Monthly newsletter (May 2019) to the company website at:

<https://www.qrp-labs.com/qcx/qcxmods/qcxwspr.html>



B. Motivation

The QRP Labs QCX CW Transceiver (QCX) is an affordable, single-band, 5 watt transceiver kit available for the 17, 20, 30, 40, 60, and 80 meter bands. When assembled, the QCX is capable of both transmitting and receiving on CW (Morse code), and it also contains a beacon mode for both CW and Weak Signal Propagation Reporter (WSPR). Of particular note, the QCX, in its existing design, is **only** capable of transmitting on the WSPR network, and it is not able to receive in WSPR mode.

One of the main attractions of the QCX is its affordability and portability. My main motivation for purchasing the QCX was that I wanted to have a dedicated, fully functional Rx/Tx beacon station on WSPR mode for a low price. My goal was to participate fully in the WSPR network as both a transmitter beacon probing propagation paths and band conditions, in addition to reporting spots of other radio operator’s transmission for automatic upload to the WSPR database via the internet. Observations

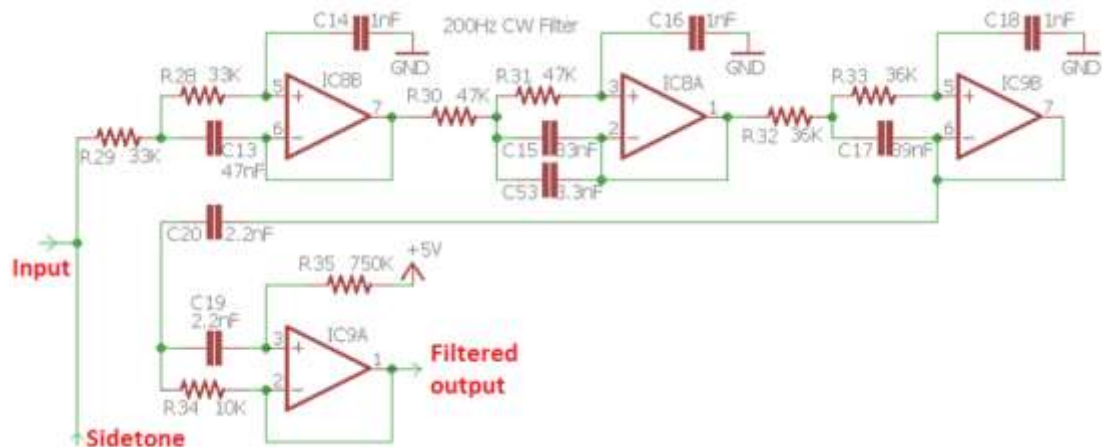
uploaded to the WSPR database, in addition to benefiting individual operators in their propagation analyses, are used by scientists to better understand the ionosphere and its interaction with other earth and space phenomena.

This project note is a summary of the modification I made to the internal circuitry of the QCX transceiver, which allow me to receive in WSPR mode. This modification was made to a completed and working QCX transceiver, and involved de-soldering some components which I had previously installed. I would like to acknowledge N6GN who helped me troubleshoot my QCX kit, and who helped me pinpoint and understand the modification described in this project note.

C. Overview of Design Specifics that Limit the Receive Capability on WSPR

The QCX Transceiver contains a 200Hz audio analogue CW filter. Operating in CW, the CW audio filter is designed to produce a 700Hz signal. As such, the CW Tx/Rx frequency range in the transceiver is a 200Hz band around this reference frequency. This CW filter, however, limits Rx in WSPR mode, which covers a frequency range of 200Hz around a center frequency of 1,500Hz.

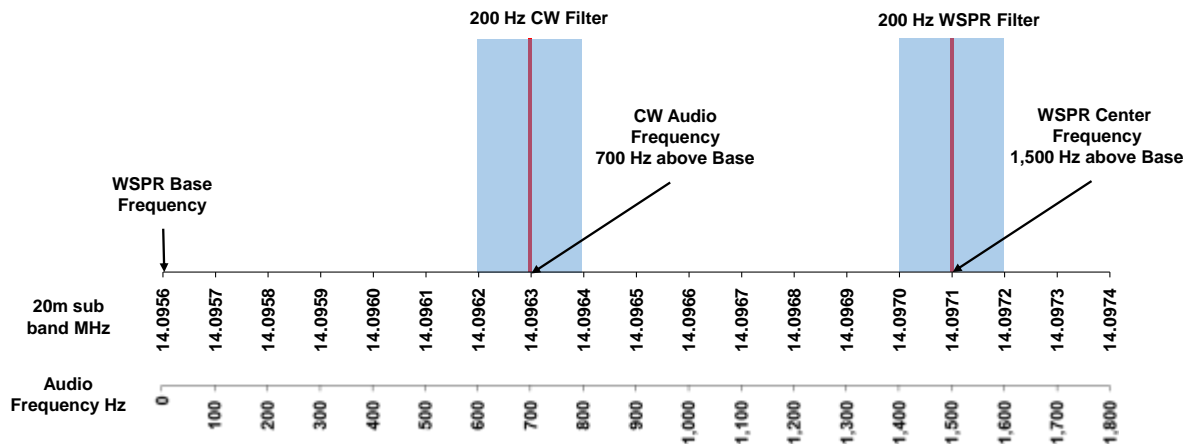
Figure 47: QCX 200Hz CW Filter



Source: QRP Labs

The above CW filter produces a tone of 700 Hz (+/- 100Hz), a common range for CW operation, which is then sent to the audio amplifier. This filter, however, does not allow higher frequency tones to pass, like those of WSPR mode at around 1,500Hz.

Figure 48: Audio frequency range of CW vs WSPR modes

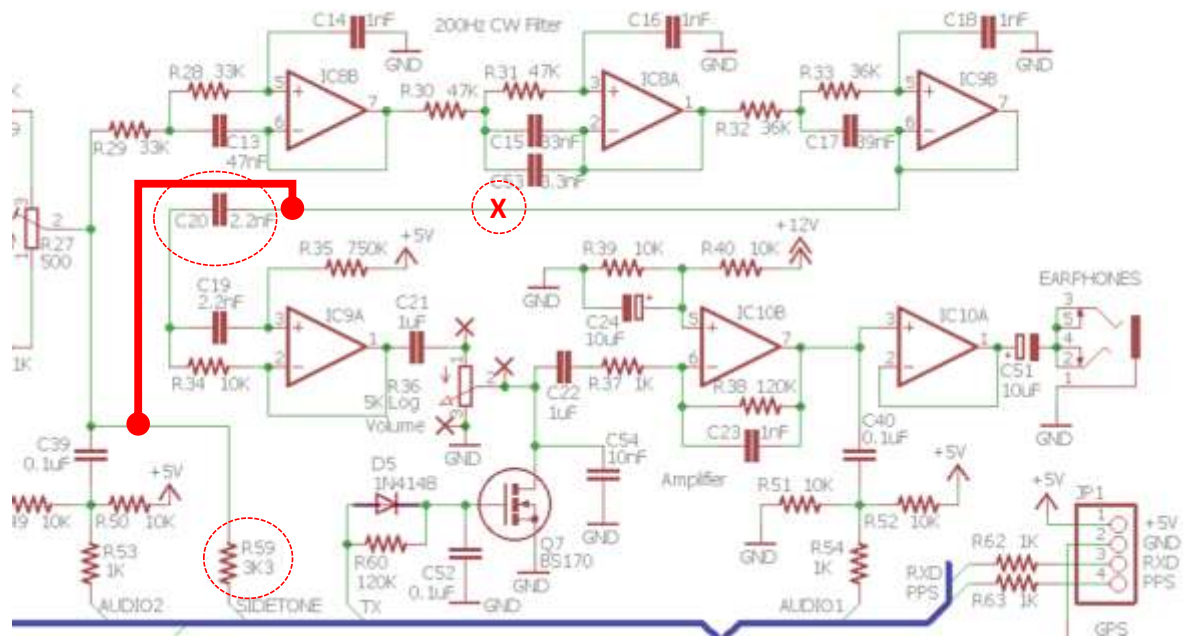




The figure above illustrates the limitation that the 200 Hz CW filter poses for WSPR Rx; the designed configuration permits a down-converted tone in a range of 600 to 800 Hz, but WSPR mode requires a tone at a higher frequency in the range of 1,400 to 1,600 Hz.

D. CW Filter Bypass Modification

The QCX version that I made this modification to is the PCB Rev 4 produced in 2018. The bypass of the CW filter and subsequent connections are detailed in the cut-out of the Schematics below.

Figure 49: CF filter bypass modification schematics

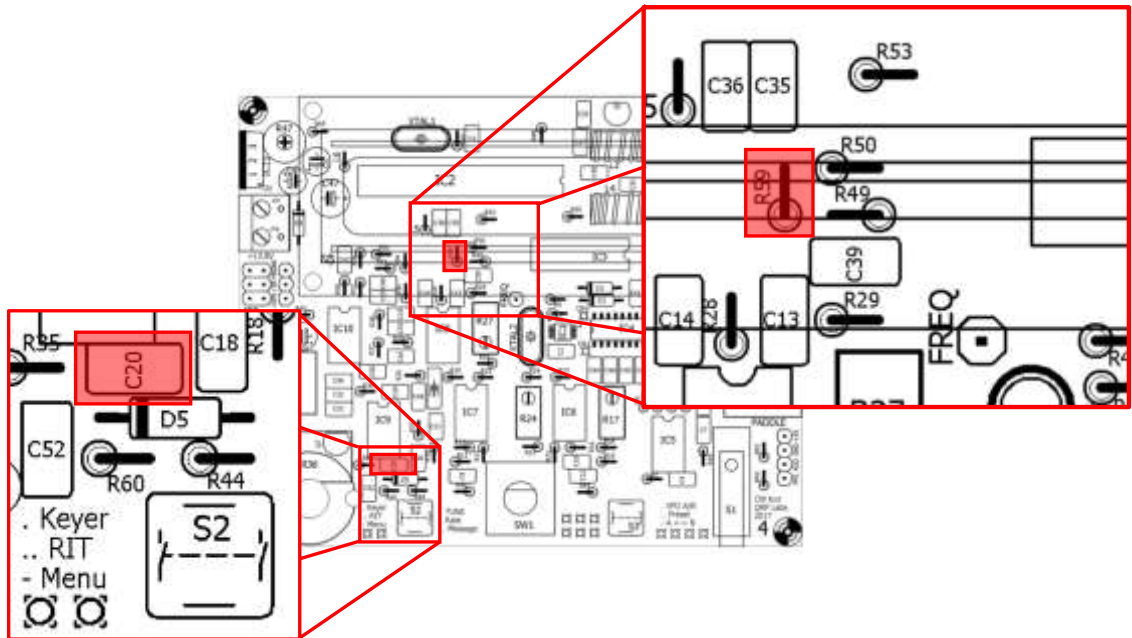


-  Bypass Modification - Connection
-  Bypass Modification - Break

Source: QRP Labs with overlay by Maxwell Moran, W3LLA

This modification bypasses the filter and reroutes the signal directly to the audio amplifier. The modification requires a break in the connection marked by the encircled “X” with the addition of a new connection between R59 (2.2nF) and C20 (2.2nF). This modification, effectively, disables the CW filter for CW receive transmission which will add noise to CW in receive mode. A switch could be added to allow the user to toggle between the fully functional Rx/Tx CW mode and the now fully functional Rx/Tx WSPR beacon mode. The figure below highlights the relevant components for this modification.

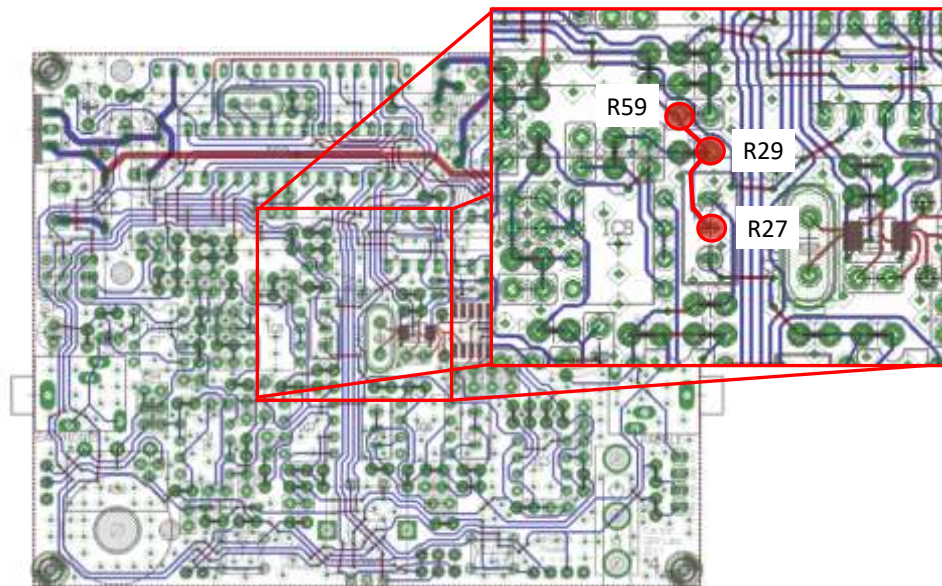
Figure 50: CF filter bypass modification - highlighted components



Source: QRP Labs with highlights provided by W3LLA

R59 is a common node into R27, the last point of audio signal prior to the CW Filter and it was chosen for its accessibility on the circuit board. R29 could have been chosen. The PCB track schematic shows the connection into R27 from both R59 and R29.

Figure 51: PCB track schematic - common nodes into R27



Source: QRP Labs with highlights provided by W3LLA

In order to perform the modification, the following steps should be made:

4. Change the orientation of the R59 Resistor by 180 degrees so the vertically positioned body wire end is attached to the PCB from the hole closest to C35, with the long wire folded over and inserted into the hole closest to C13. You will be connecting the folded over wire lead to a wire, and this orientation allows you to access the hole without interference from the resistor body.
5. Remove the right most wire from C20 from its hole entirely. This hole is the one closest to C18. This wire will not be inserted back into the hole, while the left wire will remain in its position.
6. Connect the detached right end wire from C20 to one end of a jumper wire (approx. 2 inches long).
7. Connect the other end of the jumper wire to the hole shared by the R59 long wire (e.g. the R59 hole closest to C13).

Figure 52: R59 with orientation changed (left) and jumper attached (right)



Figure 53: C20 with one end connected to PCB and the wire attached to lead (left) and completed modification (right)



Figure 54: Illustrative reception reports post modification – 2/2/2019, 20m band



Source: <http://wspr.vk7jj.com/>

VI. References

1. Stephens, Kurt and Whittington, Bill. Bringing Communications Back Down to Earth. *Signal Magazine*. 2018.
2. *The Relation of Radio Sky-Wave Transmission to Ionosphere Measurements*. Smith, Newbern. 1939, Proceedings of the Institute of Radio Engineering, pp. 332-347.
3. Jenn, David. *Ionospheric Wave Propagation - EC3630 Radiowave Propagation*. [.pdf Presentation] version 1.6.5, Monterey, California, USA : s.n. Naval Post Graduate School, Department of Electrical & Computer Engineering.
4. *Radio Propagation Prediction for HF Communications*. Mudzingwa, Courage and Chawanda, Albert. s.l. : Science Publishing Group, 27 February 2018, Communications Vol.6, No.1, pp. 5-12.
5. Silver, Ward. *The ARRL Ham Radio License Manual*. [ed.] Mark Wilson. Third Edition. Newington, CT : ARRL, 2016. Technician Manual. ISBN 978-1-62595-013-0.
6. *Radio Waves and the Ionosphere*. Pool, Ian (G3YWX). Newton, CT : The American Radio Relay League, 1999, QST Magazine.
7. *Antenna Height and Communications Effectiveness, A Guide for City Planners and Amateur Radio Operators*. Straw, Dean R. and Hall, Gerald L. [ed.] ARRL. Second Edition, Newington, CT : The American Radio Relay League, Inc., 1999, ARRL.
8. Eddy, John A. *The Sun, the Earth, and Near-Earth Space: A Guide to the Sun-Earth System*. Washington D.C. : NASA, U.S. Government Printing Office, 2009. ISBN 978-0-16-083808-8.
9. Anderson, Dave and Fuller-Rowell, Tim. The Ionosphere. *Space Environment Topics*. 1999, SE-14.
10. Greenman, Murray. <https://www.qsl.net/zl1bpu/IONO/iono101.htm>. *An Introduction to HF propagation*. [Online] [Cited: 22 12 2019.] <https://www.qsl.net/zl1bpu/IONO/iono101.htm>.
11. UCAR Center for Science Education. The Ionosphere. [Online] 2014. [Cited: 9 12 2019.] <https://scied.ucar.edu/ionosphere>.
12. Silver, Ward. *The ARRL General Class License Manual*. Eighth Edition. Newington : The American Radio Relay League, 2015. ISBN 978-1-62595-030-7.
13. Turner, Stu. D Layer Absorption. <https://hamradioschool.com>. [Online] 12 October 2015. <https://hamradioschool.com/d-layer-absorption/>.
14. HamRadioSchool.com. *D-Layer Absorption*. [Online] 12 October 2015. [Cited: 1 6 2020.] <https://hamradioschool.com/d-layer-absorption/>.
15. Department of Defense, US Marine Corps. *Antenna Handbook MCRP8-10B.11*. s.l. : Department of Defense, 2016. PCN 144000062 00.
16. NASA. Ionosphere Graphics. *NASA Goddard Media Studios*. [Online] [Cited: 27 12 2019.] <https://svs.gsfc.nasa.gov/12960>.
17. Institute of Geophysics and Planetary Physics, University of California, Los Angeles. <http://www.igpp.ucla.edu/>. [Online] [Cited: 21 12 2019.] http://www.igpp.ucla.edu/public/rwalker/ESS200C_2007_winter/The%20Ionosphere.pdf.
18. Australian Government, Bureau of Meteorology, Space Weather Services. Introduction to HF Radio Propagation. [Online] 2020. [Cited: 29 5 2020.] <https://www.sws.bom.gov.au/Educational/5/2/2>.
19. Erickson, Philip (MIT Haystack Observatory). MIT Student Cable, The Ionosphere, Shortwave Radio, and Propagation. [Online] 11 January 2019. Presentation from MIT Haystack Observatory. <https://www.youtube.com/watch?v=dRpXiwS41Z4>.

-
20. Khan, Sal. Refraction and Snell's Law. *Khan Academy*. [Online] <https://www.khanacademy.org/science/physics/geometric-optics/reflection-refraction/v/refraction-and-snell-s-law>.
21. *Understanding LF and HF Propagation*. Nichols, Steve (G0KYA) and Melia, Alan (G3NYK). Norwich : s.n., September 2009, Radio Society of Great Britain Propagation Studies Committee, p. 14.
22. Hum, Sean Victor. Ionospheric Propagation. <http://www.waves.utoronto.ca/prof/svhum/ece422/notes/20c-ionosphere.pdf>. [Online] [Cited: 7 11 2019.]
23. *Maximum Usable Frequencies for Sky-Wave Transmissions 1933 to 1973*. Gilliland, Theodore R., et al. s.l. : Department of Commerce, May 1938, Journal of Research of the National Bureau of Standards, Vol. Volume 20. Relation of vertical to oblique-incidence transmission.
24. Crombie, Douglass D. Chapter 33 - Electromagnetic-Wave Propagation. [ed.] Wendy M. Middleton and Mac E. Van Valkenburg. *Reference Data for Engineers - Radio, Electronics, Computer, and Communications*. Ninth Edition. s.l. : Elsevir, 2002.
25. Robertshaw, G.A., The MITRE Corporation. *Effective Earth Radius for Refraction of Radio Waves at Altitudes Above 1KM*. Electronic Systems Division of the U.S. Airforce Systems Command, United States Air Force. Bedford, MA : USAF, 1983. Technical Report. MTR-8915 & ESD-TR-83-219.
26. International Telecommunication Union (ITU). *Effects of Tropospheric Refraction on Radiowave Propagation - Rec. ITU-R P.834-3*. ITU. Recommendation Paper. Effective Earth radius.
27. *Definitions Of Terms Relating To Propagation In Non-Ionized Media*. International Telecommunication Union. s.l. : International Telecommunication Union, 1994. Recommendation. Recommendation ITU-R PN.310-9.
28. Thompson, Anthony, Moran, James and Swenson, George. *Propagation Effects: Ionized Media*. 2017. ISBN 978-3-319-44429-1.
29. NOAA. Ionosphere. <https://www.swpc.noaa.gov>. [Online] [Cited: 19 12 2019.] <https://www.swpc.noaa.gov/phenomena/ionosphere>.
30. National Oceanic and Atmospheric Administration National Centers for Environmental Information. *National Oceanic and Atmospheric Administration National Centers for Environmental Information*. [Online] [Cited: 19 12 2019.] <https://www.ngdc.noaa.gov/stp/cdrom/ionocd.html>. <https://www.swpc.noaa.gov/phenomena/ionosphere>.
31. The International Reference Ionosphere (IRI). [Online] [Cited: 15 12 2019.] <http://irimodel.org/#ftpweb>.
32. Breneiser, Edward. *Amateur Radio Pedestrian Mobile Handbook: Second Edition*. 2014. p. Chapter 11. ISBN 978-1-304--96221-8.
33. WSPR User Guide version 4.0. *Princeton University*. [Online] [Cited: 1 6 2020.] <http://physics.princeton.edu/pulsar/K1JT/doc/wspr/wspr-main.html>.
34. Steve Nichols, G0KYA. The Twilight Zone. *RadCom Magazine*.
35. www.movable-type.co.uk. <https://www.movable-type.co.uk/scripts/latlong.html>. [Online] [Cited: 28 03 2020.]
36. Babicki, Sasha & Arndt, David & Marcu, Ana & Liang, Yongjie & Grant, Jason & Maciejewski, Adam & Wishart, David. Heatmapper: web-enabled heat mapping for all. 2016, p. 44. gkw419. 10.1093/nar/gkw419.
38. McKeague, Charles P and Turner, Mark D. *Trigonometry 5th Edition*. s.l. : Robert W. Pirtle, 2004. ISBN 0-534-40392-1.
39. Fitzpatrick, Richard. Ionospheric Radio Wave Propagation. *University of Texas Department of Physics*. [Online] 27 June 2014. [Cited: 9 12 2019.] Relation of electron density and plasma frequency. <http://farside.ph.utexas.edu/teaching/jk1/lectures/node89.html>.

40. DeMaw, Doug (W1FB). Radio Waves and Communications Distance. *QST Magazine*. January 1985.

41. *Introduction to RF Propagation*. Seybold, John S. Hoboken, NJ : Wiley-Interscience, John Wiley & Sons Inc., 2005. ISBN-13 978-0-471-65596-1 .